Failure Pressure Prediction of Cracks in Corrosion Defects in Pipelines using eXtended Finite Element Method

by

Xinfang Zhang

A thesis submitted in partial fulfillment of the requirements for the degree of

Master of Science

In

Petroleum Engineering

Department of Civil and Environmental Engineering
University of Alberta

ABSTRACT

Pipelines are one of the safest means of oil and gas transportation. In Canada, 97% of all oil and gas production is transported by pipelines. However, their increasing age can constitute integrity concerns due to the presence of defects such as cracks, welds, dents, and corrosion. These defects can form due to coating or cathodic protection degradation or external mechanical damage. When flaws are detected in pipelines, it is extremely important to have an accurate assessment of the associated failure pressure, which would inform the appropriate remediation decision of repairing or replacing the defected pipelines in a timely manner.

There are different codes for the assessment of single defects in oil and gas pipelines. The most common codes for crack-like defect assessment are API 579 and BS 7910, there are also numerical programs such as CorLAS. The most popular methods for corrosion defects are RSTRENG, Modified B31G, and LPC methods, there are also computer programs such as CPS. Other methods such as Finite Element Method (FEM) have also been used for assessing the crack and corrosion defects. However, cracks in corrosion (CIC) represent a class of defects, for which there are no agreed-upon method of assessment, with no existing analytical or numerical models to predict their failure pressures. In general, compared to the traditional FEM, which requires extremely fine meshes and is impractical in modelling a moving crack, the eXtended Finite Element Method (XFEM) is computationally efficient while providing accurate predictions. Hence, the aim of this study was to provide a guideline for the assessment of CIC defects in pipelines using XFEM.

A parametric study was conducted in 2D to investigate the effect of different CIC parameters (initial crack depth, corrosion width, and corrosion profile) on the failure pressure and it was found

that initial crack depth had a significant influence on the failure pressure among these parameters. In addition, mesh size sensitivity was investigated successively in the elastic-only material model and elastic-plastic material model. The elastic-only material model was found to exhibit an unrealistically higher failure pressure than the elastic-plastic material model.

Several existing defect assessment methods that evaluate the failure pressure in crack and corrosion defects were reviewed. The versatility of RSTRENG, LPC, and CorLAS in predicting the failure pressure was also discussed. The study revealed that for the corrosion-only defect, the LPC method predicted the closest failure pressure to that obtained using XFEM (3.5% difference), whereas the RSTRENG method provided a more conservative prediction with 19% difference. CorLAS method provided accurate result for the crack-only defect with a 7% difference.

The finite element program ABAQUS was used to model a series of burst tests. In CIC modelling, the CIC defect was modeled as an artificial corrosion defect with an elliptical profile and a V-notch shaped crack placed in the centre of the corrosion. The failure pressure was predicted when the crack penetrated the inner surface of the pipe. Based on this criterion, it was found that for shorter cracks, the failure pressure decreased with increasing initial crack depth; when the initial crack depth exceeded 50% of the total defect depth, the CIC defect could be treated as crack-only defects, since the failure pressure for the CIC model approached that for the crack-only model for ratios of the initial crack depth to the total defect depth of 0.75 and 1. However, for longer cracks, the initial crack depth was found to have a negligible effect on the failure pressure, implying that the CIC defect could be treated as either a crack or a corrosion utilizing the available assessment methods.

PREFACE

The thesis is an original work by the author, Xinfang Zhang.

Chapter 2 of this thesis is derived from a conference paper on the proceedings of the 18th Pressure Vessel Piping Conference, Minnesota, USA, 2020.

Chapter 3 of this thesis is derived from a conference paper on the proceedings of the 2020 13th International Pipeline Conference, Calgary, Alberta, Canada.

Chapter 4 of this thesis was submitted to the International Journal of Pressure Vessels and Piping (IPVP).

DEDICATION

Dedicated to my dearest parents: Benfeng Jing and Chao Zhang, who always support me to pursue my dreams and encourage me never give up when encountering challenges in life.

ACKNOWLEDGEMENTS

I would first like to express my sincere gratitude to my supervisors, Dr. Samer Adeeb and Dr. Juliana Y. Leung, for their patience, encouragements, and continuous support throughout my master study and research.

I would like to thank Dr. Yong Li and Dr. Nobuo Maeda for being part of my examination committee and providing valuable comments.

I would also like to thank all my friends at the University of Alberta: Meng Lin, Allan Okodi, Leichuan Tan, Odin Guzman Sanchez, Sylvester Agbo, Palizi Mehrdad, Vahab Esmaeili, Qian Zheng, Saher Salama, Zixuan Cui, Wenran Zhao, Israel Molina. Special thanks to Meng Lin, and Allan Okodi for providing academic support.

This achievement would not have been possible without them.

TABLE OF CONTENTS

LIST OF TABLES

LIST OF FIGURES

LIST OF ABBREVIATIONS

AER	Alberta Energy Regulator
API	American Petroleum Institute
ASME	American Society of Mechanical Engineers
ASTM	American Society of Testing and Materials
CC	Crevice Corrosion
CCT	Critical crevice temperature
CIC	Crack in Corrosion
CPT	Critical pitting temperature
CTOD	Crack-tip opening displacement
CT	Compact Tension
CVN	Charpy V-notch impact energy
DEM	Discrete Element Method
EAC	Environmentally Assisted Cracking
EUL	Extension Under Load
FEA	Finite Element Analysis
FEM	Finite Element Method
IGC	Intergranular Corrosion
LPC	LinePipe Corrosion
LSF	Level Set Function
NACE	National Associate of Corrosion Engineers
OPS	Office of Pipeline Safety
PSL	Product Specification Levels

RA	Reduction of Area
SENB	Single Edge Notch Bend
SENT	Single Edge Notch Tension
SCC	Stress corrosion cracking
TSC	Tension Strain Capacity
UTS	Ultimate tensile strength
XFEM	eXtended Finite Element Method

LIST OF SYMBOLS

α	Material coefficient for the Ramberg-Osgood relationship
A	Cross-sectional area
A_f	Cross-sectional area at fracture
A_o	Original cross-sectional area
ΔA	Reduction of cross-sectional area
b_o	Remaining ligament
$2c$	Crack length
c_{eq}	Crack half length
D	Outer diameter of pipe
d	Defect depth
d_{cr}	Initial crack depth
d_T	Total defect depth
E	Elasticity modulus
ε	True stain
ε_p	Equivalent plastic strain
F_{sf}	Free surface factor
G	Energy release rate
G_c	Fracture energy
L_f	Gauge length at fracture
L_o	Original gauge length
ΔL	Change in gauge length
J	J integral

$J_{0.2}$	Resistance against stable crack initiation in J-integral terms at the point of 0.2 mm
J_c	Fracture toughness in J-integral determined at the point of instability
K	Stress intensity factor
K_c	Plane stress fracture toughness characterized by *K*-factor
K_I	Stress intensity factor (mode I loading)
K_{IC}	Plastic strain fracture toughness characterized by *K*-factor
l	Length of the corrosion
M_{axpe}	Maximum principal strain
M_{axps}	Maximum principal stress
M_p	Bulging factor
M_t	Folias bulging factor
n	Strain hardening exponent
n_{RO}	Strain hardening exponent of Ramberg-Osgood equations
P_f	Failure pressure
Q_f	Elliptical shape factor
R	Pipe radius
r_p	Plastic zone radius
σ	True stress
σ_{flow}	Flow stress
σ_{fs}	Failure stress
σ_h	Hoop stress
σ_{UTS}	Ultimate tensile strength
σ_{YS}	Yield strength

σ_{smts}	Specified minimum tensile strength
t	Pipe wall thickness
ν	Poisson's ratio
Y	Dimensionless geometry factor

CHAPTER 1 : INTRODUCTION

1.1 Background

Railways, roadways, airways, waterways, and pipelines are the five major transportation methods. Among these popular methods, pipelines are the most economical and feasible method for transporting oil and gas products as pipelines are usually buried underground which enables the products to be transported in a safe and confined environment. Over the past decades, pipelines have been playing an extremely important role in the onshore and offshore oil and gas development activities, which have been growing rapidly due to global energy demands [1]. Depending on the purposes, subsea pipelines can be classified as flowlines transporting oil and/or gas from subsea wells to subsea manifolds, flowlines transporting oil and/or gas from subsea manifolds to platforms, infilled flowlines transporting oil and/or gas between different platforms, and export pipelines transporting oil and/or gas from platforms to onshore [2].

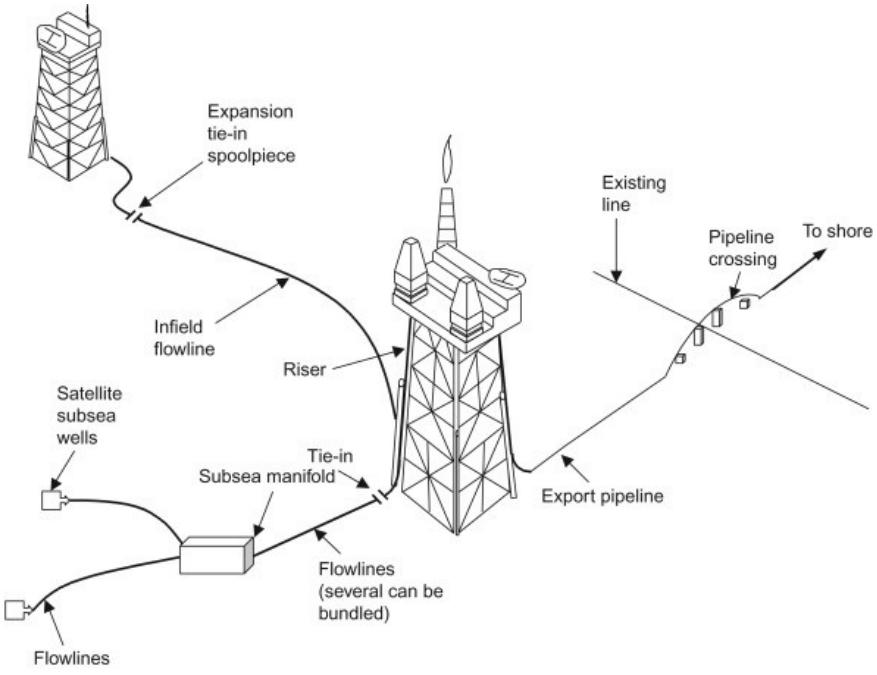

Figure 1: A typical use of offshore pipelines [2].

However, aging pipelines may experience several types of defects, which can constitute serious concerns for pipeline integrity. Cracks are one of the common defects which may result from the interaction of metallic material and a corrosive environment, could be found in the operating pipelines. Another common type of defect is corrosion. Corrosion can usually be found on the external surface of the pipe due to coating or cathodic protection degradation [3]. Cracks and corrosion sometimes occur simultaneously in the operating pipelines, representing a hybrid defect known as cracks in corrosion (CIC), as shown in Figure 2 [4].

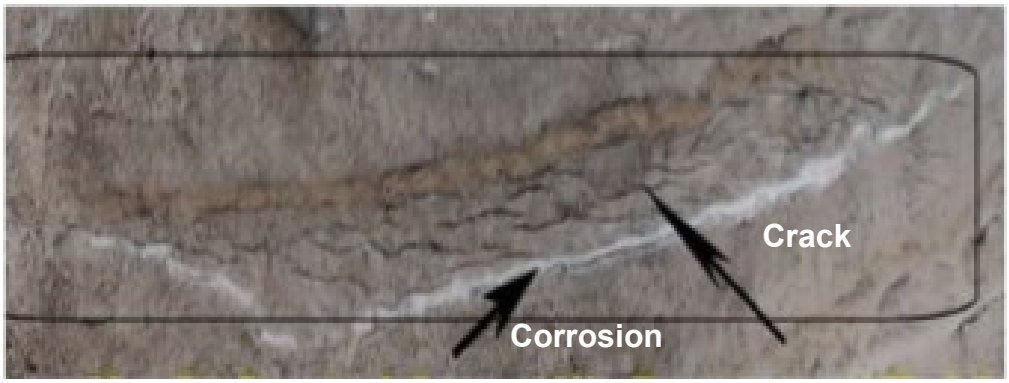

Figure 2: Example of CIC in pipelines [4].

According to a report released by Alberta Energy Regulator (AER), there were 416 pipeline incidents in 2018 and some experts believe that this problem could be addressed if the pipeline had been properly maintained [5]. An accurate prediction of the failure pressure is extremely important in the integrity assessment of oil and gas transmission pipelines and will enable the operators to make appropriate repair or replacement decisions [6]. In addition, such knowledge is necessary to make a prudent decision on the safe dig pressure in case there is a need to replace the defect.

1.2 Problem Statement

For modeling single defects, different equations or codes are available to evaluate the associate failure pressures. For example, the RSTRENG [7], and LPC methods [8,9] are commonly used to evaluate corrosion defects; API 579 [10], BS 7910 [11], and CorLAS software [12] have been used successfully for assessing crack defects in pipelines.

At present, the failure pressure for a hybrid defect, such as CIC, has not been studied extensively and usually cannot be directly addressed with the current available assessment methods. Other researchers chose to simplify the treatment of CIC defect as either corrosion-only or crack-only single-defect with an equivalent depth and length, enabling the utilization of the available assessment methods.

Hybrid defects, such as CIC, can be challenging to model using traditional Finite Element Method (FEM); the method is considered expensive and tedious, as it requires fine meshes around the crack tip region. In modelling of a moving crack, automatic adaptive mesh refinement is needed as the crack propagates to conform to the geometric discontinuity. Hence, using FEM to predict the failure pressure is relatively difficult, since it requires extremely fine meshes and is impractical for modelling crack propagation.

The extended finite element method (XFEM), however, provides an alternative that is computationally efficient: the mesh is independent of the geometry and there is no need to re-mesh the crack domain upon crack propagation [13-17], as shown in Figure 3.

While XFEM is ubiquitous in many applications, it has not gained traction in pipeline application as of yet. Hence, considering that there is a lack of assessment methods to predict the failure pressure of pipes with CIC defects, the current research focuses on the application of XFEM technique for addressing the limitation discussed above toward and assessing the feasibility of XFEM technique for analysing CIC defects.

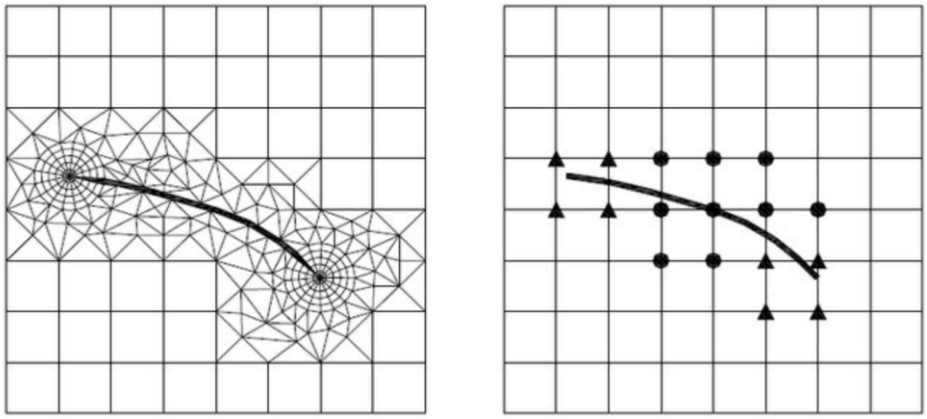

(a) **(b)**

Figure 3: Illustrative sketches of (a) a conforming FEM mesh; (b) a non-conforming XFEM mesh [18].

1.3 Objective of Thesis

The overall objective of this thesis was to investigate the application of the extended finite element method, as implemented in ABAQUS [19], for constructing hybrid CIC defects in 2D and 3D. Both maximum principal strain and fracture energy are considered as damage parameters for analysis. These XFEM modelling results are analysed to examine failure behavior under different conditions and to infer guidelines for assessing or predicting failure pressures corresponding to hybrid CIC defects in oil and gas pipelines. Specific objectives of this research are to:

(i) Conduct a parametric study on CIC defects in pipelines in 2D, which includes the mesh size sensitivity analysis and the investigation of the effects of different CIC parameters (initial crack depth, corroded area width, and corrosion profile) on the failure pressure.

(ii) Investigate the effectiveness of RSTRENG, LPC, and CorLAS in predicting the failure pressure, calibrate XFEM models using the experimental results from Bedairi et al. [13], and examine the effect of initial crack depth on the failure pressure using X60 material.

(iii) Using the calibrated model from (ii) to predict failure pressures for two additional sets of experimental data from Ma et al. [20]. After that, examine the effect of initial crack depth on the failure pressure with various defect geometries and material properties to provide general guidelines for assessing CIC defects.

1.4 Organization of Thesis

This thesis is a paper-based thesis, organized as follows:

Chapter 1 describes the background of cracks in corrosion defects on pipelines.

Chapter 2 covers a comprehensive literature review of pipes such as the specification of pipes, mechanical properties, types of pipeline failures, and existing methods for assessing crack and corrosion in oil and gas pipelines.

Chapter 3 presents a parametric study on pipelines in 2D which includes the examinations of mesh size sensitivity and the effects of different CIC parameters on the final failure pressures in

elastic-only material model and elastic-plastic material model. The difference of these two models are also discussed. Chapter 3 is from a research paper that was previously published in the proceedings of the America Society of Mechanical Engineers (ASME) 2020 Pressure Vessel Piping (PVP) Conference.

Chapter 4 presents a study to calibrate the XFEM damage parameters and validate the numerical finite element analysis models that are suitable for accurately predicting the failure pressure of 3D CIC defects using the experimental data from Bedairi et al. [13]. Chapter 4 is from a research paper that was previously published in the proceedings of the America Society of Mechanical Engineers (ASME) 2020 International Pipeline Conference (IPC).

Chapter 5 presents the methodology and the results of validating XFEM models using the full-scale burst test data from Ma et al. [20], the investigation of the effect of initial crack depth on the failure pressure, and the dependence of the failure pressure on the defect lengths. Chapter 5 is from a research paper that was submitted to the International Journal of Pressure Vessels and Piping (IPVP).

Chapter 6 summarizes the key findings through this research and recommends the future work.

All references in this study are given after Chapter 6.

1.5 Novelties and Contributions

This work presents a comprehensive assessment of CIC defects in pipelines using XFEM technique. The XFEM predictions are validated against the results from experiments conducted on vintage X42, X52, and X60 pipes. Although numerous studies have been carried out to predict the failure pressure of pipes with cracks, corrosion and CIC defects, all the previous work was either focusing on modelling CIC defects in traditional FEM or modelling crack-only defects in XFEM.

To the best of the authors' knowledge, this work is the first rigorous attempt to conduct a parametric study on CIC pipelines and predict the failure pressure of pipes containing CIC defects utilizing XFEM.

CHAPTER 2: LITERATURE REVIEW

2.1 Introduction of Pipelines

2.1.1 Grades of Pipes

In oil and natural gas industry, pipes are usually classified by the American Petroleum Institute (API) Spec. 5L (2018) [21]. There are two basic Product Specification Levels (PSL) of standard technical requirements for seamless and welded pipes known as PSL 1 and PSL 2. The standard quality of PSL 2 is more stringent than PSL 1 since PSL 2 contains additional chemical composition and testing requirement. For an API 5L pipe, the yield strength identifies as the number that follows the X in the material designation, for example, an API 5L X60 implies having a minimum yield strength of 60 KSI.

2.1.2 Failures of Pipelines

Pipelines are usually made of steel and buried underground. The interaction between the pipe and the surrounding environment may result in the presence of several types of defects such as crack, corrosion, dents, welds, and gouges (Figure 4 [22]). These defects may pose severe threats to the structural integrity of the pipeline as they are connected with environmental damages, human causalities, and injuries. The following parts present the general information about each defect.

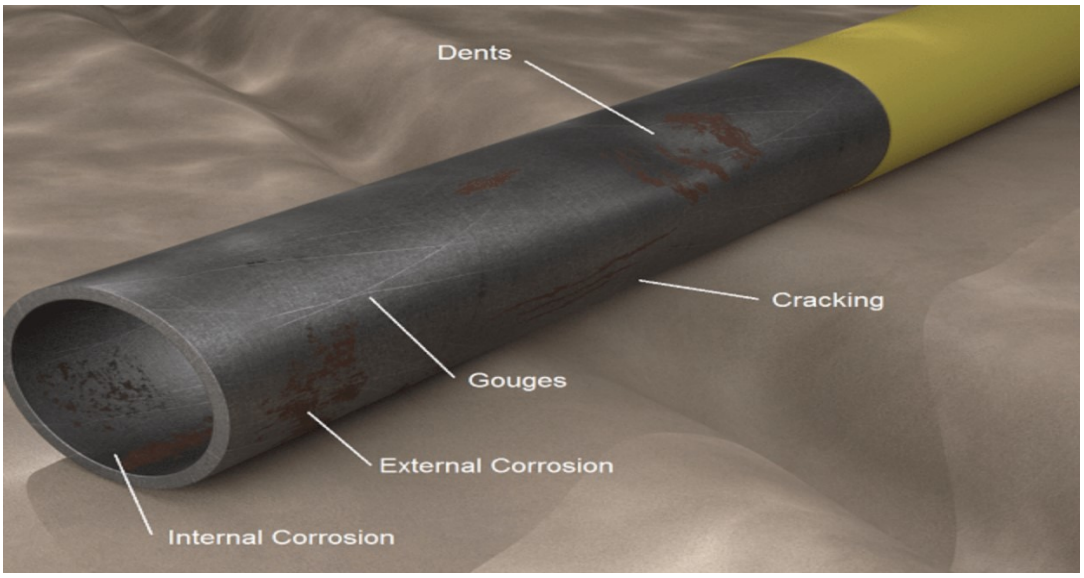

Figure 4: Common defects in pipelines [22].

- **Crack**

Cracks can be developed during the manufacturing, fabrication, and installation process which may result from the interaction of susceptible metallic material and a corrosive environment (Figure 5 [23]). A crack defect, as a severe defect, can cause high stress concentration field around the crack tip leading to a reduction in pipe strength. There are several important factors that affect the pipe strength: internal pressure, pipe diameter, ultimate tensile strength, yield strength, and fracture toughness. The morphology is highly variable based on the cause of the crack, the pipeline material and the environment. Cracks can initiate on the external pipeline surface and grow in both depth and length directions.

Figure 5: A photograph of a crack in a pipe [23].

- **Corrosion**

Corrosion is one of the common forms of defects in the operating pipelines. Corrosion can naturally occur on a pipe that is unprotected and exposed to the environment. In general, external corrosion can occur in a pipe due to coating failure. Corrosion can also occur on the interior of the pipe resulting from contaminants in the products. Depending on the corrosion morphology, corrosion can be categorized into general corrosion and localized corrosion.

(1) Crevice corrosion (localized corrosion)

Crevice corrosion (CC), also called concentration cell corrosion, usually initiates by the concentration difference of ions or dissolved gases in an electrolytic solution. Crevice corrosion is dangerous as it occurs in areas that are invisible which makes the identification procedures of crevice initiation and propagation challenging [24]. It is one of the common types of corrosion

found in pipe flanges. CC can be affected by some critical factors such as the material (alloy composition and structure), crevice type (metal-to-metal and metal-to-non-metal), geometry of crevice (gap size and depth), and the environment (oxygen and pH) [25]. There are several methods to evaluate the material's resistance to the crevice corrosion. For example, the critical crevice temperature (CCT) in accordance with the ASTM Standard G48-03 can be used to assess the crevice corrosion resistance of a metallic material, where the CCT is the minimum temperature required to produce crevice corrosion. There is also computer software such as CRA-Compass can be used to predict crevice corrosion. Figure 6 [26] depicts an oil and gas pipeline under crevice corrosion.

Figure 6: Crevice corrosion [26].

(2) Stress corrosion cracking (localized corrosion)

Stress corrosion cracking (SCC), a type of Environmentally Assisted Cracking (EAC), is commonly the result of joint action of a corrosive environment and tensile stress. The pipeline failure rate due to SCC is not high, approximately 1/100 of incidents reported to Office of Pipeline Safety (OPS), however, the existence of SCC makes the pipes more susceptible to third party damage [27]. In general, there are two forms of SCC found on buried steel pipelines, known as high-pH SCC (9-13) and near neutral-pH SCC (5-7), where pH meaning the environment at the crack location. Fracture mechanics models and excavation data can be utilized to evaluate the pipelines subjected to SCC [28]. Moreover, several methods can be used to prevent the occurrence of SCC such as applying cathodic protection, inhibitors, coatings, and changing the alloy.

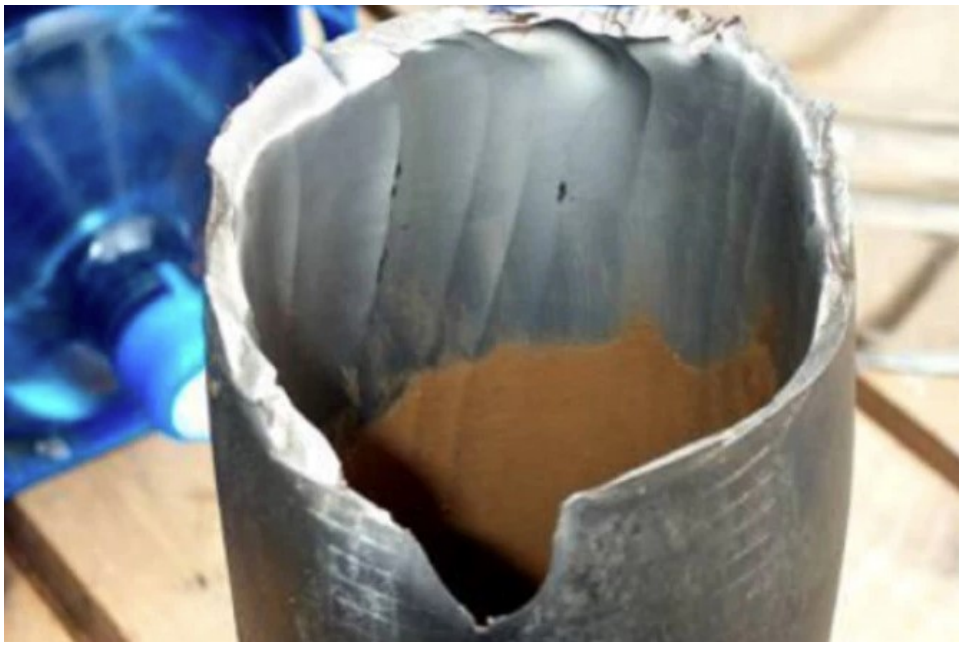

Figure 7: Stress corrosion cracking [26].

(3) Pitting corrosion (localized corrosion)

Pitting corrosion is a deep, narrow corrosive attack in a localized area and can usually be found on passive metals and alloys like aluminum alloys and stainless steel. Pitting corrosion is normally initiated by the environment that may contain aggressive materials such as chloride, hypochlorite, and bromide [29]. It can perforate extremely rapidly through the wall thickness of a metal and can be prevented by using cathodic protection and higher alloys. According to a study conducted by the National Association of Corrosion Engineers (NACE), there were more than 90% of corrosion failures of pipelines in U.S. between 1970 and 1984 were due to pitting corrosion [30]. The critical pitting temperature (CPT) in accordance with the ASTM Standard G48-03 are used to assess the pitting corrosion resistance of a metallic material.

Figure 8: Pitting corrosion [26].

(4) Erosion corrosion (localized corrosion)

Erosion corrosion occurs when the metal is exposed to the high velocity of flowing liquid, as shown in Figure 9 [31]. It is not as common as the other forms of corrosion faced by oil and gas industry. Several parameters such as temperature, wetness and pH value can affect erosion corrosion process [32]. For example, copper alloys are attached at a flow rate of 1m/s, whereas stainless steels can tolerate a flow rate of 20 m/s. Erosion corrosion can be prevented by reducing the fluid velocity and using corrosion inhibitors. The remaining life can be predicted using a powerful software known as FAC-Compass.

Figure 9: Erosion corrosion [31].

(5) Intergranular corrosion (localized corrosion)

The intergranular corrosion (IGC) is a form of corrosion attack that follows the grain boundaries path of the crystal grains in metal, resulting in loss of strength. It mainly occurs on the passive metals like other forms of localized corrosion. The Intergranular corrosion can be prevented by using low carbon grade of stainless steels.

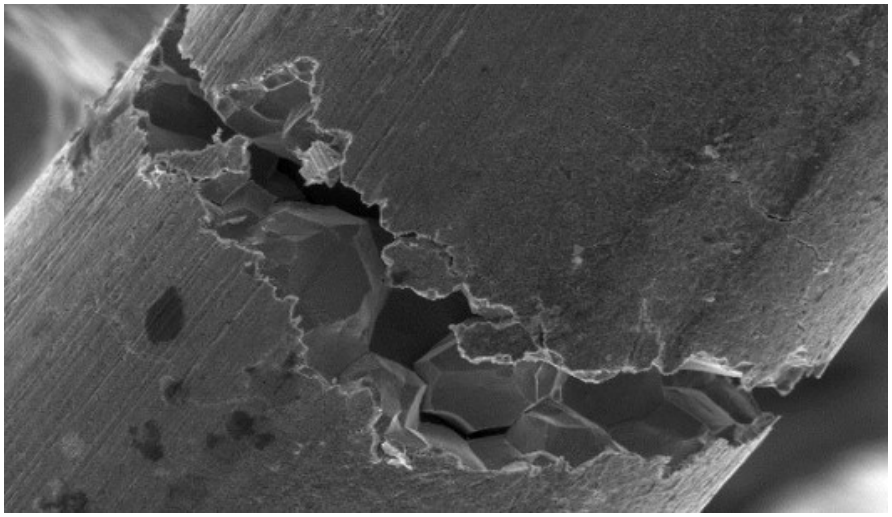

Figure 10: Intergranular corrosion [33].

(6) Uniform / General corrosion

Uniform corrosion, the most common type of attack, is the thickness reduces at a uniform rate over the whole metal surface. From a technical standpoint, uniform corrosion is not an insidious form of corrosion as it can be relatively easy to measure or predict the penetration rate using laboratory results [34]. The popular methods used to mitigate uniform corrosion are using the coatings, corrosion inhibitors and cathodic protection.

Figure 11: Uniform / General corrosion [35].

- **Dents**

Dents are the permanent plastic deformation of the pipe wall which causes an inward distortion of the pipe cross-section and can be formed due to the interaction with the excavation equipment and rock during the pipeline service period. Dents can be formed alone or may form along with other defects such as cracks and gouges. Depending on the curvature of the dents, they can be classified into two categories: kinked dents and smooth dents. The important parameters relating to dents are dent depth, pipe geometry, curvature profile, and pressure. Figure 12 [36] shows a photograph of a dent in the pipeline.

Figure 12: Photograph of a dent in the pipeline [36].

- **Gouge**

A gouge defect is considered as a severe defect in a pipe and may occur on the pipe surface during the pipe installation process. Gouges sometimes are treated as crack-like defects for the assessment of failure pressure. A study by Alang et al. [37] investigated the effect of gouge defects on the

failure pressure using Finite Element Analysis (FEA) and it was found that the gouge length has a significant effect on the failure pressure, in particular, the failure pressure decreases when the gouge length increases.

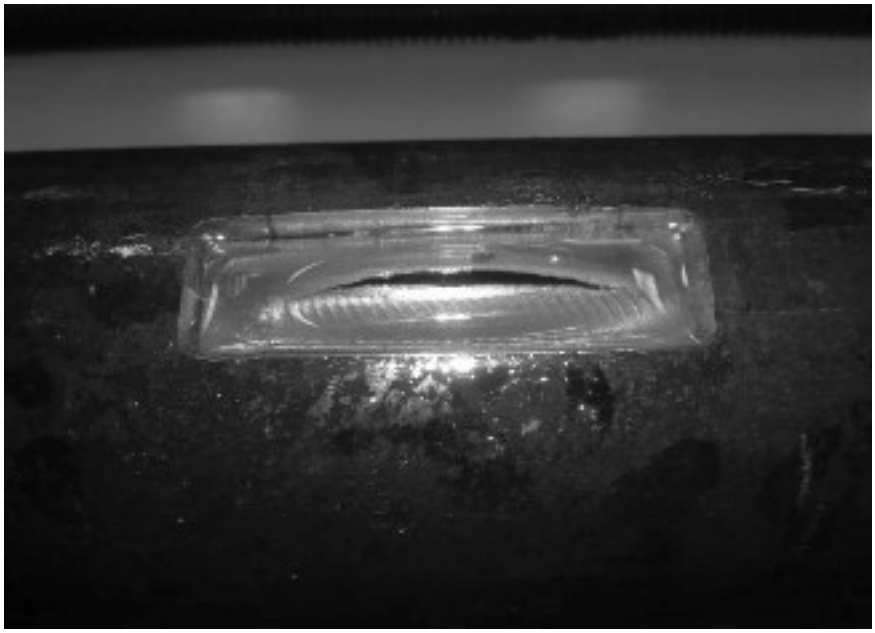

Figure 13: Photograph of a pipe with gouge [37].

2.2 Mechanical Properties of Steel

2.2.1 Modulus of Elasticity and Poisson's Ratio

Modulus of Elasticity (*E*), also called Young's modulus, is a measure of the stiffness of an elastic material and it is determined as the slope of the elastic portion of a stress-strain curve. Stiffer material has a higher value of elasticity modulus which can also be calculated by using the following equation:

$$E = \frac{tensile\ stress}{tensile\ strain} = \frac{\sigma}{\epsilon} \quad (1)$$

Poisson's ratio (υ), also known as the Poisson coefficient is the ratio of the traverse contraction strain to axial strain and it is another elastic property that used to measure the stiffness. For different materials, the Poisson's ratio can vary between -1 to 0.5. For line pipe steel, the Poisson's ratio is 0.3.

$$\upsilon = -\frac{d\epsilon_{trans}}{d\epsilon_{axial}} = -\frac{d\epsilon_x}{d\epsilon_y} \tag{2}$$

2.2.2 Yield Strength

The yield strength is usually defined as the stress at which the metallic material begins to deform plastically. Beyond this point, the deformation will be permanent or irreversible. The yield strength of a material is determined using tensile tests from which the material stress-strain curves are obtained (Figure 14 (a)). However, some metallic materials although yield gradually, making the yield point difficult to define on the stress-strain curve, in such case, there are several methods to determine the yield strength. For example, the offset method and Extension Under Load (EUL) method, defined by the ASTM E8/E8M-11 standard [38], are widely used for metallic materials. Specifically, the offset method involves drawing a line is drawn that is parallel to the specified modulus portion with a distance of 0.2% along the x-axis, as shown in Figure 14 (b). The yield point will be taken as the stress when the plastic strain equals to 0.2% (offset yield point). In the EUL method, the yield strength is determined as the stress corresponding to a total strain of 0.5% (Figure 14 (c)).

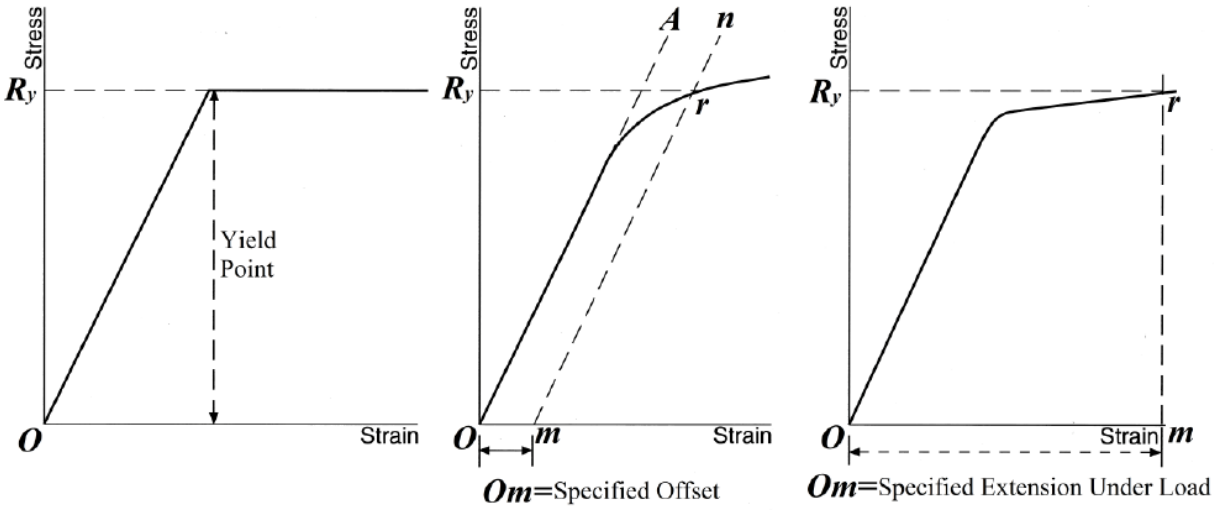

(a) Yield point method **(b) Offset method** **(c) EUL method**

Figure 14: Stress-strain diagrams showing of yield strength determination [39].

2.2.3 Ultimate Tensile Strength

The ultimate tensile strength (UTS) is the maximum stress that a material can resist before failure. The UTS can be determined at the highest point on the stress-strain curve or calculated using the following equation:

$$\sigma_f = \frac{P_f}{A_o} \tag{3}$$

Where σ_f is the tensile strength, A_o is the cross-sectional area, and P_f is the load applied on the material. The UTS is an important engineering parameter for brittle materials such as ceramics because there is no yield point. It should be noted that for metallic material, the UTS is larger than the yield strength by a factor of between 1.1 to 5 [40].

2.2.4 Fracture Toughness

Fracture toughness describes the capability of a material to resist crack propagation and the value is usually determined by a parameter known as stress intensity factor (K). The stress intensity factor is calculated as a function of the applied stress, the specimen geometry, and the crack size, which can be expressed by the following equation [41]:

$$K_I = Y\sigma\sqrt{\pi a} \tag{4}$$

Where K_I is the stress intensity factor under mode I loading (Figure 15 [42]), σ is the applied load (MPa), a is the crack depth (m), and Y is a factor that depends on the specimen geometry and the loading mode. A crack is expected to grow when K_I reaches the fracture toughness defined by K_{IC} which is considered a material property. Depending on the sample size and testing conditions, the same material may have different values for K_{IC}. Therefore, a fracture toughness test is suggested to measure the plain-strain fracture toughness, determined by one of the fracture toughness parameters such as the stress intensity factor (K), the energy release rate (G), the J-integral (J) and the crack-tip opening displacement (CTOD). The most common methods to investigate the resistance to crack propagation are the single edge notch bend (SENB) and the compact tension (CT) specimens [43].

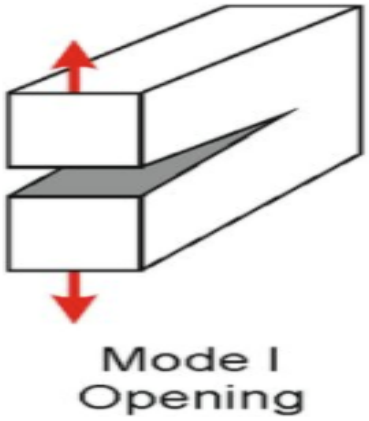

Figure 15: Mode I loading [42].

2.2.5 Elongation and Reduction of Area

The ductility of the material can be established by measuring the elongation and reduction of area (RA), and both of them are expressed as a percentage. The elongation is defined as the change in the gauge-length divided by the original length of a test specimen. The reduction of area is obtained from the tensile test and it is defined as the difference between the original cross-sectional area and the final area divided by the original area of a sample. The two above ductility parameters can be expressed by the following equations [44]:

$$Percent\ Elongation = \frac{L_x - L_o}{L_o} \tag{5}$$

Where L_x is the final length and L_o is the original length.

$$Percent\ recution\ of\ area = \frac{A_o - A_f}{A_o} \tag{6}$$

Where A_o is the original cross-sectional area and A_f is the cross-sectional area after fracture.

2.3 Current Assessment Methods

2.3.1 Crack Defect Assessment

- **Modified NG-18 equation**

The Modified NG-18 equation is a semi-empirical model that incorporates the flow stress and Charpy fracture energy (CVN) to calculate the failure pressure of pipelines containing crack-like defects. The Modified NG-18 equation was proposed by Kiefner [45] and released in 2008 due to the conservatism in the original version which was introduced in the late 1960s by Hahn [46].The original NG-18 equation incorporates the flow stress and fracture toughness to calculate the failure pressure using the following equation [4]:

$$K_c^2 = \left(\frac{EC_v}{A}\right)^2 = \frac{8}{\pi} c_{eq} \times {\sigma_{flow}}^2 \times lnsec\left(\frac{\pi \times M_P \sigma_h}{2\sigma_{flow}}\right) \quad (7)$$

where A is the fracture area of the Charpy specimen, M_P is the bulging factor, σ_h is the hoop stress, c_{eq} is half of the crack length, and the failure pressure can be calculated as follows:

$$P_f = \frac{2t}{D\pi M_P} \sigma_{flow} \cos^{-1}\left(\frac{1}{e^{\frac{E\pi C_V}{8AC_{eq}\sigma_{flow}^2}}}\right) \quad (8)$$

The main limitation of the original NG-18 equation is that it tends to underestimate the failure pressure of long, shallow defects and low-toughness materials [45]. A modification to the NG-18 equation was made to overcome this limitation, and the failure stress (σ_{fs}) in the modified version can be expressed as follows [47]:

$$\sigma_{fs} = \frac{\left(\frac{\sigma_{flow}}{M_P}\right)\cos^{-1}(e^{-x})}{cos^{-1}(e^{-y})} \tag{9}$$

where

$$x = \left(\frac{12\frac{CVN}{A_0}E_\pi}{8c{\sigma_{flow}}^2}\right) \tag{10}$$

$$\mathrm{y} = \mathrm{x}\left(1 - \left(\frac{d}{t}\right)^{0.8}\right)^{-1} \tag{11}$$

and

$$M_P = \frac{1-\frac{a}{tM_t}}{1-\frac{a}{t}},\ M_t = \sqrt{1 + 1.255\left(\frac{C_{eq}^2}{Rt}\right) - 0.0135\left(\frac{c_{eq}^4}{R^2t^2}\right)} \tag{12}$$

where CVN is the upper shelf energy, M_t is the Folias bulging factor, E is the Young's modulus, $2c$ is the crack length, and A_0 is the cross-sectional area. The flow stress is defined by: $\sigma_{flow} = \sigma_{YS} + 68.95$ MPa. It is important to note that the "flow stress", as the name implies, is a measure of the stress at which the metallic material yields or flows. The "flow stress" does not have a distinct definition and is taken as a value between the yield and ultimate strength of the metallic material. The failure pressure can be expressed by:

$$P_f = \sigma_{flow}\frac{2t}{D}\left(\frac{1-\frac{A}{A_0}}{1-\frac{A}{A_0 M_p}}\right) \tag{13}$$

- **CorLAS**

CorLAS is a computer program developed by CC Technologies [48] that is widely used by many pipeline operators to predict the failure and remaining life of pipelines containing crack-like defects. In the model, a crack-like defect is evaluated using two criteria: flow stress and fracture toughness. Flow stress is defined by either $\sigma_{flow} = \sigma_{YS} + 69.8$ MPa or $\sigma_{flow} = \frac{\sigma_{YS}+\sigma_{UTS}}{2}$, where σ_{UTS} is ultimate tensile strength. The following equation is used to compute the J-integral value [49]:

$$\mathrm{J} = Q_f F_{sf} a[\frac{\sigma^2 \pi}{E} + f_3(n)\epsilon_p \sigma] \quad (14)$$

Q_f, F_{sf}, σ, n, ϵ_p are, respectively, the elliptical shape factor, free surface factor, applied stress, strain hardening exponent, and the equivalent plastic strain, while f_3(n) is a function developed by Shih and Hutchinson [50]. The applied values of J are computed iteratively and compared with the critical value, J_c. Failure pressure is predicted when $J = J_c$. The final failure pressure is the least of the predicted failure pressures using the two criteria.

- **FE Modelling of Cracks**

The Finite element method (FEM) is a numerical method used to solve complicated problems by discretizing them into smaller elements. The concept of finite element could be traced back to the early of 1940s and the term of "finite element method" was first used in a published paper by Clough in 1960 [51]. FEM has been widely used to study crack defects and evaluate the failure pressure; for example, Bedairi et al. [13] modelled four 200 mm long cracks of 38%, 47%, 48%, and 51%WT with semi-elliptical and uniform depth profiles to predict the onset of the crack

propagation using FEM. The crack was modelled as a blunt notch with a specific root radius, which was approximately 1/1000 of the plastic zone size, r_p. The plastic zone size can be calculated as a function of toughness (K_I) [52]:

$$r_p = \frac{1}{2\pi}\left(\frac{K_I}{\sigma_{YS}}\right)^2 (1-2v)^2 \quad (15)$$

The predicted results were conservative against the experimental data with an average error of 5.35% for the semi-elliptical profile and 19.64% for the uniform depth profile. Their studies revealed the influence of the crack profile on the failure pressure prediction. Although FEM could provide less conservative results, this approach required expensive computational cost.

- **XFEM Modelling of Cracks**

Due to the limitation on simulating discontinuity, such as a crack, in the framework of FEM, Belytschko et al. [53] proposed an advanced method with a displacement function based on the concept of partition of unity in 1999, and this technique is known as the extended finite element method (XFEM). For modelling weak discontinuities, such as inclusions and biomaterial interface, the level set function (LSF) and signed distance functions are used; for modelling strong discontinuities, like cracks and faults, the Heaviside function, $H(x)$, is used. The XFEM displacement approximation, $\boldsymbol{u}$, can be written as:

$$\boldsymbol{u} = \sum_{I=1}^{N} N_I(x)[\boldsymbol{u_I} + H(x)\boldsymbol{a_I} + \sum_{a=1}^{4} Fa(x)\,\boldsymbol{b_I^a}] \quad (16)$$

where N_I (x) is the Ith nodal shape function, $\boldsymbol{u_I}$ is the nodal displacement vector, $\boldsymbol{a_I}$ is the enrichment nodal degree of freedom vector over the interior of the crack, $\boldsymbol{b_I^a}$ and $Fa(x)$ are the nodal enriched degree of freedom vector at the crack tip and the associated elastic asymptotic crack-tip functions.

The XFEM-based cohesive segments approach was employed here to simulate the crack initiation and propagation in Abaqus/Standard [54]. This approach is based on a traction-separation behaviour [54]. The fracture process is defined by a traction-separation model, consisting of a damage initiation criterion and a damage evolution law. The damage initiation criterion is satisfied when the maximum principal stress, M_{axps}, or the maximum principal strain, M_{axpe}, at the cohesive zone tip reaches to a user-defined critical value. The damage evolution law, usually defined by the energy that is dissipated due to fracture, G_c, or the effective displacement at complete failure. The M_{axps} or M_{axpe} controls the crack initiation, whereas G_c controls the crack propagation.

Several studies were undertaken to evaluate the crack propagation using the XFEM technique, with different damage parameters. However, the damage parameters were simply estimated from either tensile strength or CVN in the past studies [55-58]. Recently, the damage parameters were calibrated and validated from experiments. For example, Lin et al. [59] predicted tensile strain capacity (TSC) of circumferentially cracked API X52 pipeline using the damage parameters of the maximum principal stress and the fracture energy. In their work, the two damage parameters were calibrated and verified using the experimental results from eight full-scale tests. They concluded that G_c = 900 N/mm and M_{axps} = 750 MPa would give the most satisfactory results. In addition, Okodi et al. [47] predicted the failure pressure of three API X60 pipe specimens having

longitudinally rectangular-shaped cracks, with M_{axpe} and G_c as damage parameters. The calibration was based on a set of single edge notched tension (SENT) test data and burst tests data. It was shown that the fracture energy obtained using SENT test data (150 N/mm) was much higher than the one obtained using burst test data (23.3 N/mm), whereas the fracture strains were similar using the two approaches. Furthermore, four analytical models (CorLAS, Modified Ln-Sec, API 579 level 2B FAD, and BS7910 Level 2B FAD) were used for predicting failure pressure of pipe specimens and their results were compared with XFEM predictions. Although every analytical model was able to give a reasonable prediction, XFEM was shown to be the most accurate and effective method with a mean prediction error of -1%.

2.3.2 Corrosion Defect Assessment

- **RSTRENG**

The RSTRENG, a method that is based on the NG-18 equation, is considered as a less conservative method in predicting the failure pressure of corrosion-only defects compared to other assessment methods, such as the Modified B31G approach. RSTRENG considers the actual corrosion geometry using the effective area to calculate the remaining strength [13].

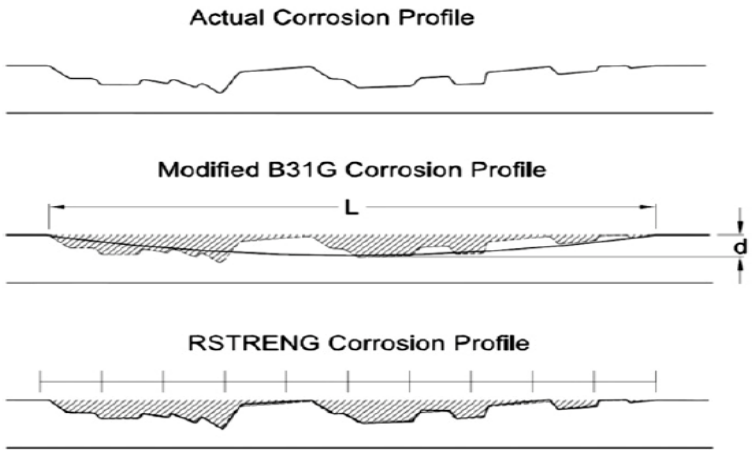

Figure 16: Corrosion profiles in RSTRENG and Modified B31G [13].

It should be noted that this method assumes a corrosion-like defect and does not explicitly account for interactions associated with CIC defects. The failure pressure can be expressed by [60]:

$$P_f = \left(\frac{t}{R}\right)\sigma_{flow}\left[\frac{1-\frac{d}{t}}{1-\frac{d}{tM_t}}\right] \tag{17}$$

where D is the pipe diameter, d is the defect depth, R is the pipe radius, and t is the wall thickness.

$$\sigma_{flow} = \sigma_{YS} + 69.8\text{MPa} \tag{18}$$

when $\frac{l^2}{Dt} \leq 50$, the Folias bulging factor, M_t is given by:

$$M_t = \sqrt{1 + 0.6275\frac{l^2}{Dt} - 0.00337\frac{l^4}{(Dt)^2}} \tag{19}$$

for $\frac{l^2}{Dt} > 50$,

$$M_t = 0.032\frac{l^2}{Dt} + 3.3 \tag{20}$$

- **LPC**

LinePipe Corrosion (LPC) criterion incorporates the specified minimum yield strength (σ_{smts}) of the pipe material to predict the failure pressure due to corrosion defects. This method was

developed by Fu et al. [8] and has been discussed by Hassanien and Adeeb [9]; it can be written as the following equation:

$$P_f = 2\sigma_{smts}\left(\frac{t}{D-t}\right)\left[\frac{1-\frac{d}{t}}{1-\frac{d}{tM_t}}\right] \tag{21}$$

where,

$$M_t = \sqrt{1 + 0.31(\frac{l^2}{Dt})} \tag{22}$$

It is worth noting that the LPC assumes the corrosion shape to be rectangular, and Eq.21 may be invalid for high-grade steel pipelines, since the LPC model was calibrated using pipeline grades up to X65.

- **FE Modelling of Corrosion**

Among all the numerical methods that have been implemented, the finite element method is the most commonly used approach to predict the failure pressure of a corrosion defect. For example, Mok et al. [61] built simplified 2D and 3D models with actual material properties and defect geometry in order to predict the failure pressure. The material properties were taken from tensile test data and the failure was predicted to occur when the strains in the corrosion ligament started to increase asymptotically. The FEM prediction results were accurate compared to the experimental data with an average 5% error.

Several 3D finite element analyses were conducted by Cronin [62] who modelled single corrosion pits and long grooves using the stress-based criterion. The onset of failure was predicted when the von Mises stress exceeded the ultimate tensile strength. It was found that the FEM predictions had an error of -0.18%, with a standard deviation of 8.45%. Ma et al. [63] also used FEM to predict failure pressure of high-grade strength steel pipelines with corrosion defects and investigate the effects of corrosion depth and length on the failure pressure. The results indicated that the failure pressure decreases as the ratio of pipe diameter to wall thickness ($\frac{D}{t}$) increases and it also decreases as $\frac{l}{\sqrt{D \cdot t}}$ increases.

2.3.3 Cracks in Corrosion (CIC) Defect Assessment

FEM has been widely used in many past studies for predicting the failure pressure of crack in corrosion defects. Bedairi et al. [13] validated the numerical finite element analysis models with experimental rupture tests to predict the failure pressure of pipes with artificial CIC defects, where a CIC defect was considered as a corrosion defect with a flat bottom and a crack defect with uniform depth. It was found that the failure pressure predictions for CIC defects using FEM analysis were conservative with a mean error of 17.4%; in addition, their results showed that the prediction error increased with crack depth.

Cronin et al. [64] built several FEM models in 3D to predict the failure pressures of various CIC defects with a fixed initial total defect depth but different crack and corrosion depths. The failure pressure for crack-only defects and corrosion-only defects were investigated separately. Failure was predicted to occur when the J-integral value exceeded the critical value ($J_{0.2} = 120\ \mathrm{kJ/m^2}$). NG-18, FAD, and FE approaches were used to calculate the failure pressure. It was found that the

failure pressure of a CIC defect would vary between that of a crack-only defect and a corrosion-only defect with uniform depth.

In summary, numerous studies have used FEM for the assessment of the failure pressure associated with crack, corrosion and cracks in corrosion defects in pipelines, however, FEM requires re-meshing for discontinuities such as cracks, which makes this method complicated and inefficient. Recently, some efforts have been made to investigate the application of XFEM, with M_{axpe} or M_{axps}, and G_c as the damage parameter for analysis of the crack propagation. For example, Lin et al. [59] used stress-based criterion to simulate the TSC of circumferentially cracked pipeline and Okodi et al. [47] used strain-based criterion to predict the failure pressure of longitudinally cracked pipeline.

However, the assessment of CIC defect in pipelines has not been studied in XFEM. Hence, there is a need to explore the applicability of XFEM on assessing the cracks in corrosion defects and predicting the failure pressure in pipelines. In this research, M_{axpe} and G_c were selected as XFEM damage parameters to characterize the fracture process, which were calibrated based on the experimental results from literature [13,20].

CHAPTER 3: A 2D PARAMETRIC STUDY ON CIC IN PIPELINES[1]

3.1 Introduction

In this chapter, the objective is to study the applicability of XFEM in predicting the failure pressure of CIC defects in 2D. In particular, a parametric study on CIC pipelines was conducted which included the mesh size sensitivity and the effects of different CIC parameters on the final failure pressure were examined. For simplicity, only half of the pipe was modelled assuming symmetry around the horizontal plane. The pipe dimensions were chosen randomly with no connection to the real pipe. A CIC defect was placed at the exterior of the pipe. The corroded area was assumed to be semi-elliptical, and the crack was simulated as a longitudinal crack. Failure criterion was satisfied when the crack has propagated to the last element. Several models were built in which the length and width of the elements at the crack tip were changed to conduct the mesh size sensitivity. An optimum mesh size was determined and was applied subsequently in several other models to study the impacts of initial crack depth (d_{cr}), corrosion width, and corrosion profile (semi-rectangle and semi-ellipsoid) on the failure pressure.

[1] A version of this chapter has been published in the conference proceedings:

Zhang, X.F., Okodi, A., Tan, L.C., Leung, J.Y., and Adeeb, S. Forthcoming. (2020). Failure pressure prediction of crack in corrosion defects in 2D by using XFEM. PVP 2020-21046, Proceedings of the 18th Pressure Vessel Piping Conference, Minnesota, USA.

3.2 Methodology

3.2.1 Elastic-only Material Model

1) 2D Model Set up

For simplicity, only half of the pipe was modelled assuming symmetry around the horizontal plane. The outer diameter (OD) of the pipe was taken as 260 mm with a 10 mm wall thickness. A CIC defect was placed at the exterior of the pipe. To assess the mesh size sensitivity, the width of the corroded area was taken as 10 mm and the combined depth of the corrosion and the crack was fixed at 2.5 mm. The corroded area was assumed to be semi-elliptical, and the crack was simulated as a longitudinal crack.

Initially, the pipe was assumed to be composed of an elastic isotropic material, with the Young's modulus and the Poisson's ratio of 200 GPa and 0.3, respectively. Later, an elastic-plastic analysis was performed and the differences between the two models were compared. The geometric non-linearity option was chosen for the analysis step. The following random values were assigned to the XFEM parameters: The maximum principal strain was set as 0.005; damage evolution was controlled by the fracture energy of 10 N/mm. ABAQUS also requires the input of a viscosity coefficient, and the recommended default value of 1e-5 was used. In order to improve the model accuracy, the initial and the maximum increment size in the step definition section were set as 0.005, the minimum increment size was equal to 1e-15, and the maximum number of increments allowable was 1000.

A pressure of 120 MPa was applied to the inner surface of the pipe. The failure criterion was satisfied when the crack has reached the last element, and the corresponding pressure was recorded

as the failure pressure. The boundary conditions were chosen to allow for pipe expansion due to variation in the internal pressure. The boundary conditions on the left and right horizontal edges were set as: U2 = UR3 = 0 and U1 = U2 = UR3 = 0, respectively (Figure 17 (a)). Partitions were created in order to control the generated mesh for different regions around the crack (Figure 17 (b)).

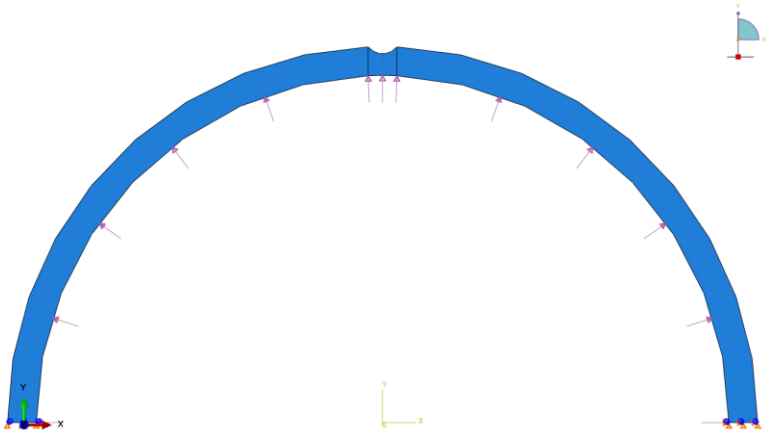

(a)

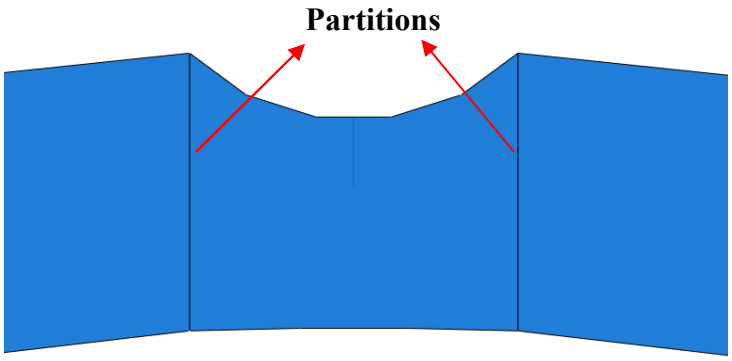

(b)

Figure 17: Schematic of modelled pipe showing (a) boundary conditions and loading; (b) the location of partitions.

2) Mesh Size Sensitivity Study

The objective is to find the optimum mesh size, such that further mesh refinement would not have a discernible effect on the failure pressure. Several models were built in which the length and width of the elements at the crack tip were changed and the effect on the failure pressure was investigated. However, after the mesh width size was decreased to around 1.2 mm, the crack would propagate only one element through the thickness direction; therefore, a damping effect was added, and an automatic stabilization scheme was specified in the step definition section using the default value to stabilize the model with the specify dissipated energy fraction and the ratio of stabilization to strain energy were set as 0.0002 and 0.05, respectively. In addition, the tolerance in the "Maxpe Damage" step was increased from 0.05 to 0.5.

3) CIC Parameters

After determining the optimal mesh size, additional models are constructed to investigate the combined effect of the crack and corrosion defects on the failure pressure. The following are the parameters used to define the CIC defect (Figure 18):

- Total defect depth, d_T, from the crack tip to the outer surface of the pipe if undamaged. ($d_T = d_c + d_{cr}$). An initial value of d_T was set at 5 mm or 50% of wall thickness in this section.
- Corrosion depth, d_c, from the bottom of the corroded area to the outer surface of the pipe if undamaged.
- Initial crack depth, d_{cr}, from the crack tip to the bottom of the corroded area.
- Remaining wall thickness, b_o, from the crack tip to the inner surface of the pipe. An initial value of b_o was fixed at 5 mm or 50% of wall thickness.

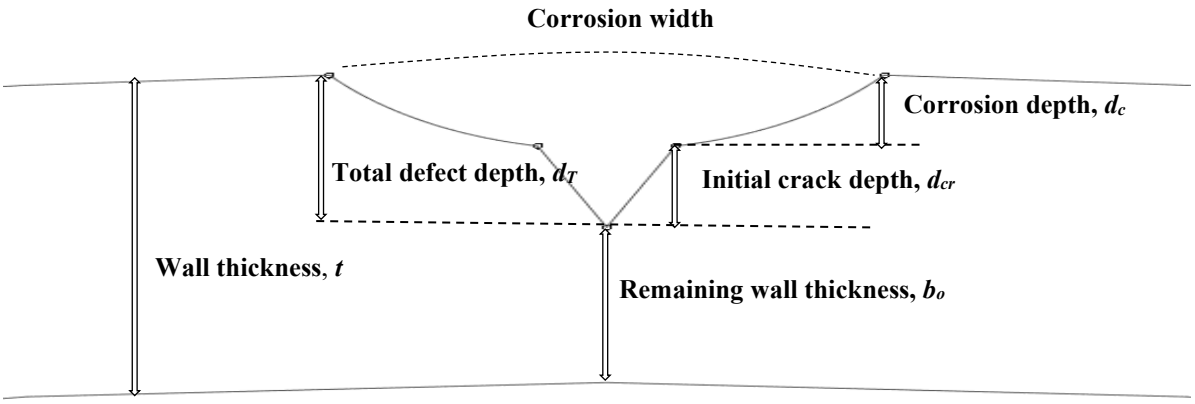

Figure 18: The definition parameters of a CIC defect.

Depth of the Crack

The dependence of failure pressure on the initial crack depth was investigated in this part. The total defect depth, d_T, was fixed at 5 mm. The width of the corroded area was fixed at 10 mm. The depth of the crack varied from 0.5 mm to 5 mm and the depth of the corrosion varied accordingly. Five models were built with different crack and corrosion depths.

Width of the Corroded Area

The total initial defect depth remained at 50% of the wall thickness, the depths of the corrosion and the crack were both fixed at 2.5 mm. The width of the corroded area was taken as 10 mm, 15 mm, and 20 mm (three models).

Corrosion Profile

In this part, the initial depths of each of the corrosion and the crack remained at 2.5 mm. The width of the corroded area was fixed at 10 mm. The profile of the corroded area was changed. Two

models (one with semi-rectangular profile and one with semi-elliptical profile) were built (Figure 19).

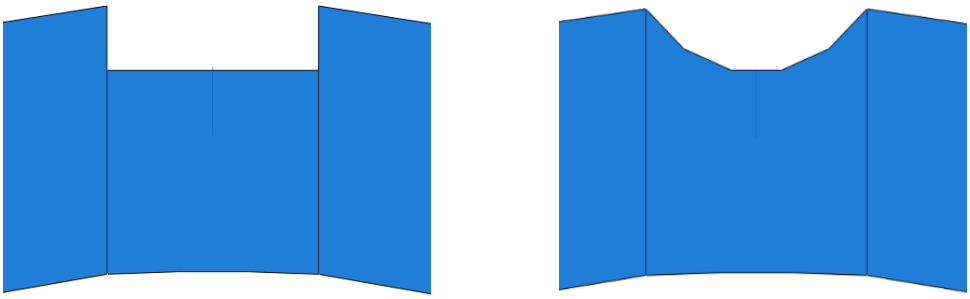

Figure 19: Chosen corrosion profiles.

3.2.2 Elastic-plastic Material Model

1) 2D Model Set Up

Similar to the elastic material model, only half of the pipe was modeled. The outer diameter (OD) of the pipe was taken as 260 mm with a 10 mm wall thickness. The pipe was simulated as an elastic-plastic isotropic material with the Young's modulus and the Poisson's ratio equal to 200 GPa and 0.3, respectively. Material properties derived from [20] were used and semi-elliptical corrosion profile were assumed. The stress-strain data were obtained using the Ramberg-Osgood equation (Eq. (23)).

$$\epsilon = \frac{\sigma}{E} + \left(\frac{\sigma}{\mathrm{H_{RO}}}\right)^{\frac{1}{n_{\mathrm{RO}}}} \tag{23}$$

where

$$n_{\mathrm{RO}} = \frac{1+1.3495\left(\frac{\sigma_{YS}}{\sigma_{UTS}}\right)-5.3117\left(\frac{\sigma_{YS}}{\sigma_{UTS}}\right)^2+2.9643\left(\frac{\sigma_{YS}}{\sigma_{UTS}}\right)^3}{1.1249+11.0097\left(\frac{\sigma_{YS}}{\sigma_{UTS}}\right)-11.7464\left(\frac{\sigma_{YS}}{\sigma_{UTS}}\right)^2} \tag{24}$$

and

$$H_{\mathrm{RO}} = \frac{\sigma_{UTS} \exp(n_{\mathrm{RO}})}{n_{\mathrm{RO}}^{n_{\mathrm{RO}}}} \tag{25}$$

Ma et al. [20] employed these values: σ_{YS} = 289 MPa and σ_{UTS} = 413 MPa. The true stress-strain curve obtained using Eq. (23) is shown in Figure 20. The maximum principal strain of 0.005 and the fracture energy of 10 N/mm were used as the XFEM damage parameters. Same symmetric boundary conditions as in the previous section were applied to the model. Internal pressure was applied to the inner surface of the pipe during the analysis (Figure 21 (a)). Failure was predicted to occur when the crack has reached the last element. Partitions were created in order to locally refine the mesh around the crack, while a coarser mesh was implemented in other regions (Figure 21 (b)).

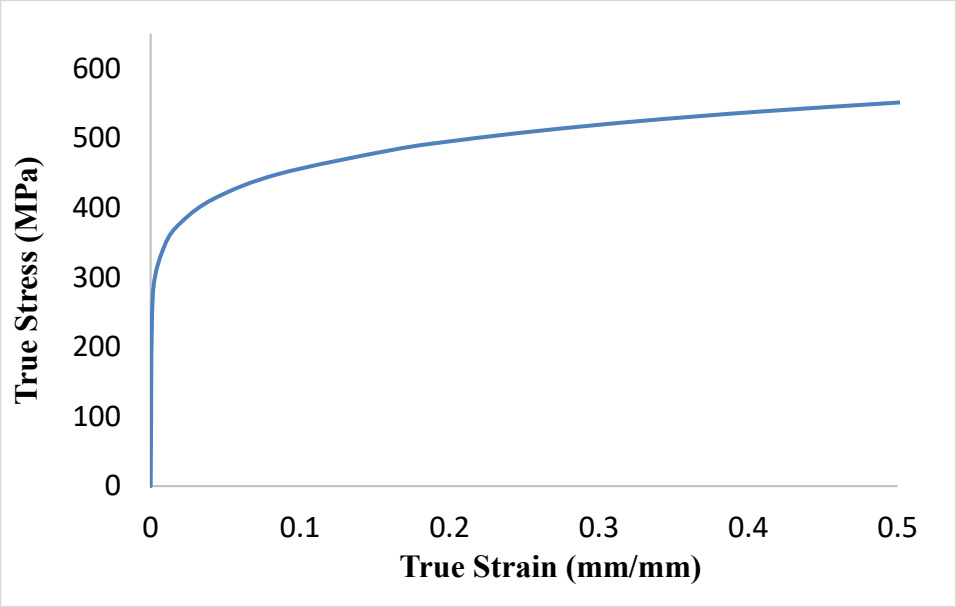

Figure 20: A stress-strain curve constructed from a Ramberg-Osgood equation in API 579, adapted from Ma et al. [20].

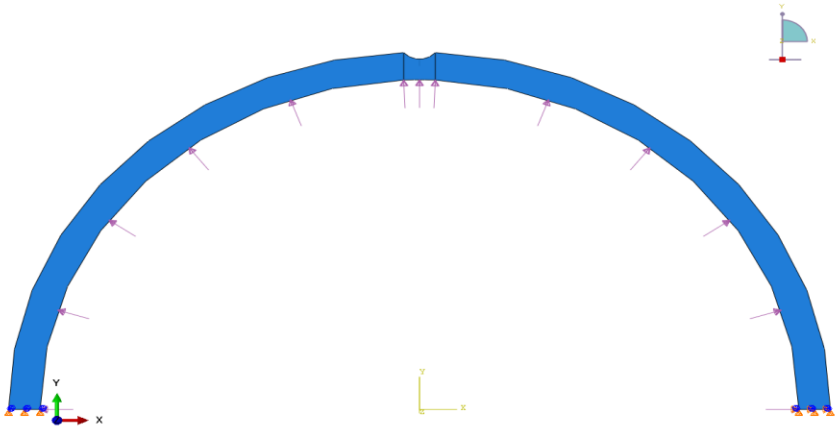

(a)

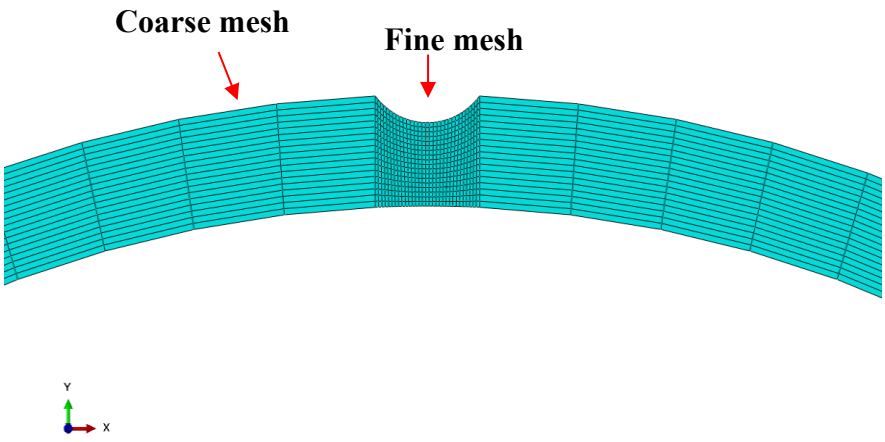

(b)

Figure 21: (a) Half model of the pipe with boundary conditions and loading; (b) model mesh detail.

2) Mesh Size Sensitivity Analysis

The effect of mesh size on the numerical stability was examined by changing the mesh size in two directions. Several models were built in which the length and width of the mesh elements, namely l_h and l_t at the crack tip were changed and the effect on the failure pressure was investigated. In

the beginning, mesh length size was fixed at 1.64 mm, and then the mesh width size was varied until there is no discernible effect on the failure pressure upon further mesh refinement.

3) CIC Parameters

Additional models (using the optimal mesh size) were constructed to investigate the effects of various CIC parameters on the failure pressure prediction for an elastic-plastic model.

3.3 Results and Discussion

3.3.1 Typical Behavior

Typical 2D crack in corrosion defects models were shown in Figure 22. The mesh sizes were selected randomly before mesh size sensitivity analysis. As shown in Figure 22 (a), the first six layers were penetrated by the original (initial) XFEM crack. As the pressure increased, the crack increased in size as it traversed through the additional elements. Figure 22 (b) shows the extent of crack opening when the step time has reached 0.19 and beyond; the crack propagated through the pipe wall thickness direction until the crack tip has penetrated the inner surface of the pipe (Figure 22 (c)).

The failure pressure (P_f) was calculated as the input load pressure times the step time when the crack has reached the final element. However, in this case, the value of the increment jumped from 0.0001 to 0.2 at the final step time (Figure 22 (c)), therefore, in order to get more accurate results, the actual final step time was taken as 0.2058, where the last element was intact (Figure 22 (d)).

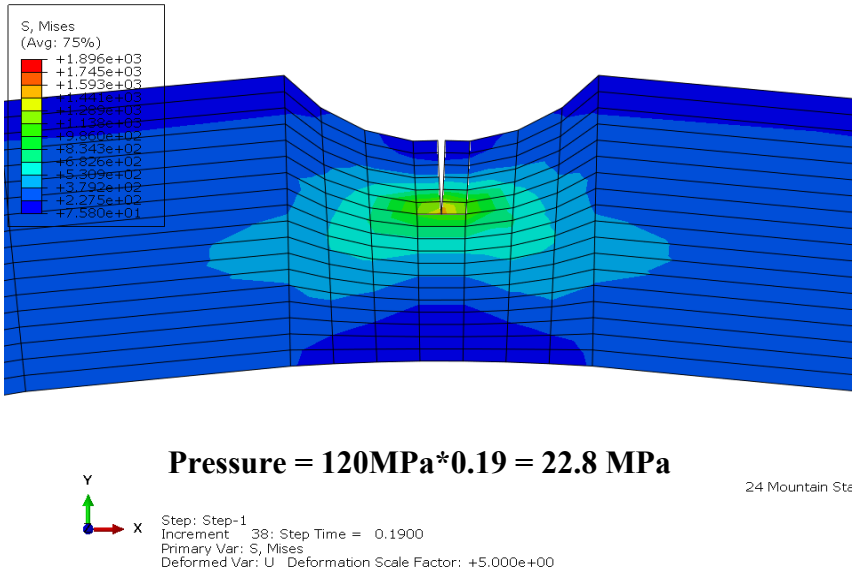

Pressure = 120MPa*0.19 = 22.8 MPa

(a)

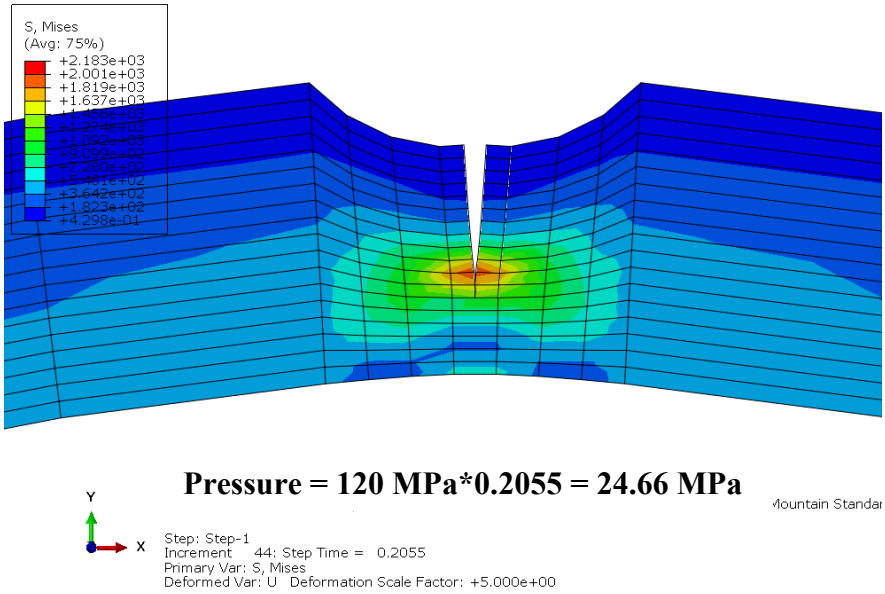

Pressure = 120 MPa*0.2055 = 24.66 MPa

(b)

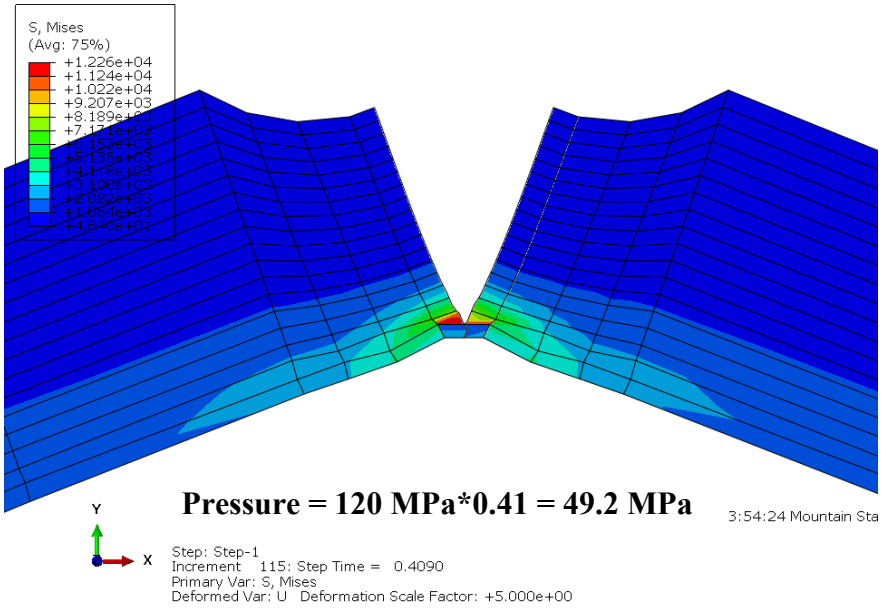

(c)

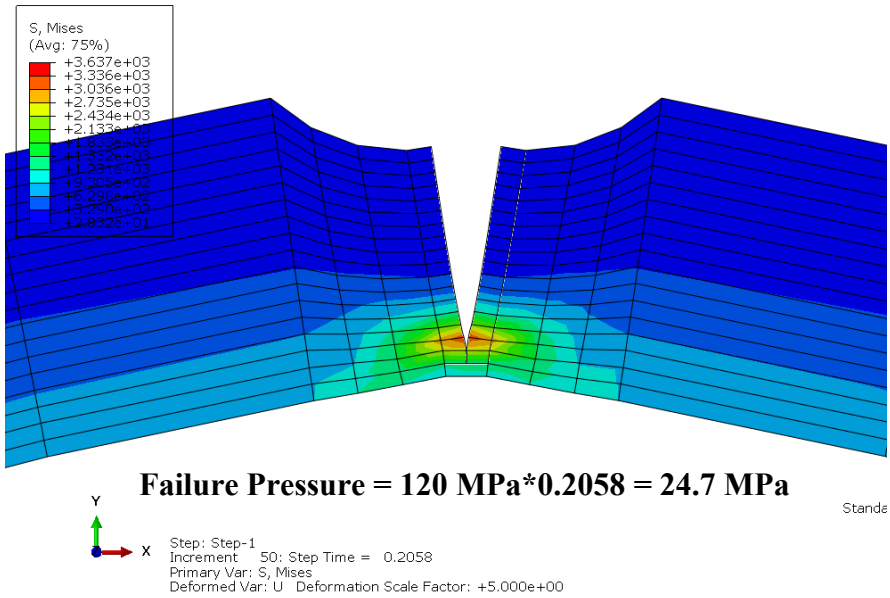

(d)

Figure 22: The numerical modelling results showed (a) right before the crack propagated through the first element; (b) an intermediate step; (c) the final step; (d) the step where the last element was intact.

3.3.2 Mesh Size Sensitivity Analysis

1) Elastic-only Material Model

Figure 23 shows a scatter plot of the predicted failure pressure with decreasing mesh width size l_t at a constant mesh length l_h, while Figure 24 shows the variation of the failure pressure with decreasing mesh length l_h at a constant mesh width size l_t.

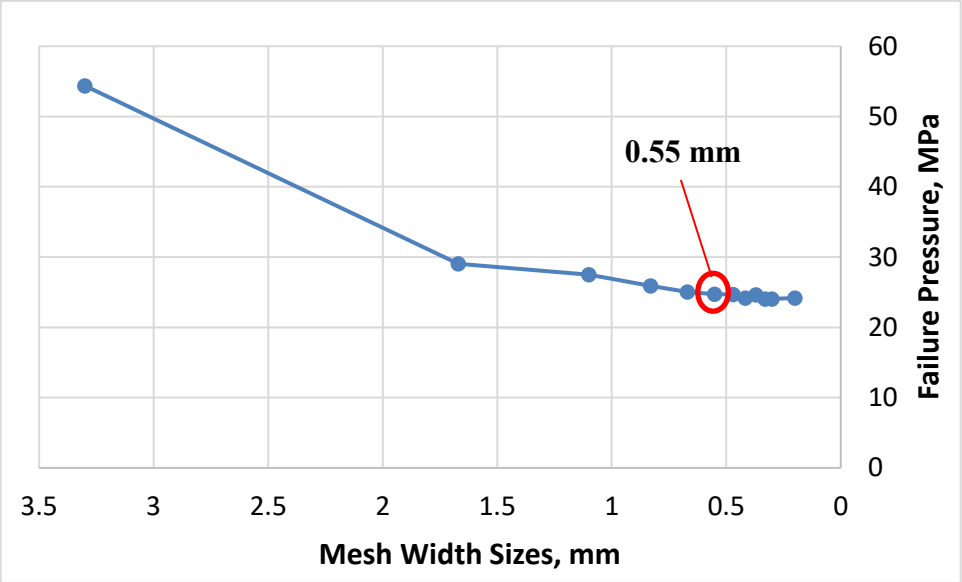

Figure 23: Failure pressure for different mesh width sizes for elastic-only material model.

In Figure 23, it was observed that when l_h was fixed at 1.64mm, the failure pressure stabilized after l_t has reached a value of around 0.55mm.

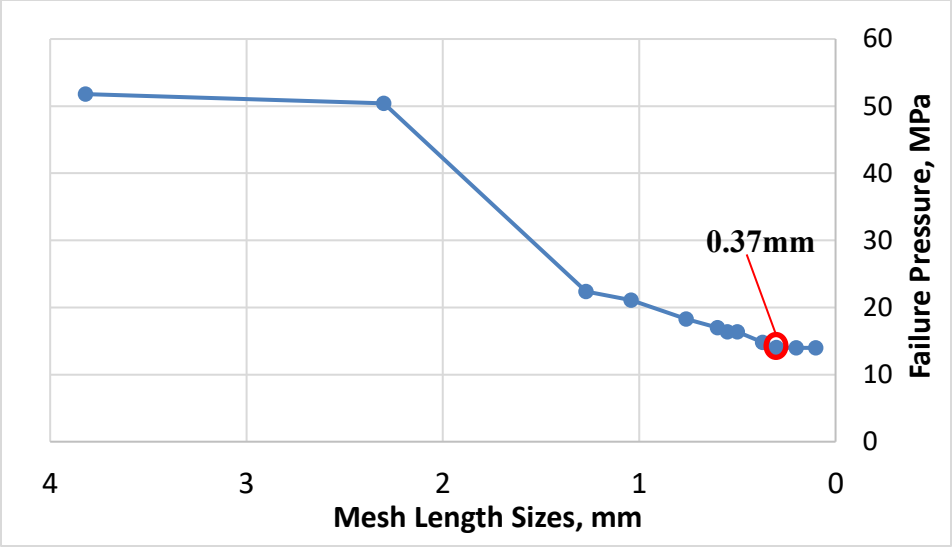

Figure 24: Failure pressure for different mesh length sizes for elastic-only material model.

Figure 24 indicates that the failure pressure stabilized after l_h has reached a value of around 0.37 mm. There, it was deduced that the failure pressure would stabilize when the mesh size was $l_h \times l_t$ = 0.37 mm × 0.55 mm. In consideration of computational efficiency, this mesh size was chosen as the optimum for calculating the effect of the CIC parameters on the failure pressure.

2) Elastic-plastic Material Model

Figure 25 below shows the variation of the failure pressure with decreasing the mesh width size l_t at a constant mesh length l_h, while Figure 26 shows the variation of the failure pressure with decreasing the mesh length l_h at a constant mesh width size l_t.

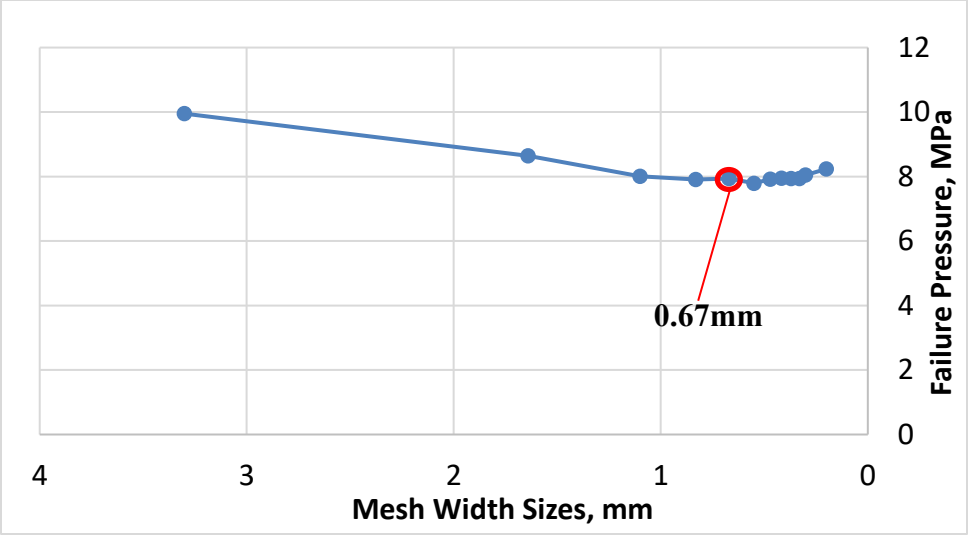

Figure 25: Failure pressure for different mesh width sizes for elastic-plastic material model.

When l_h was fixed at 1.64 mm, it was observed that the failure pressure stabilized after l_t has reached a value of around 0.67 mm.

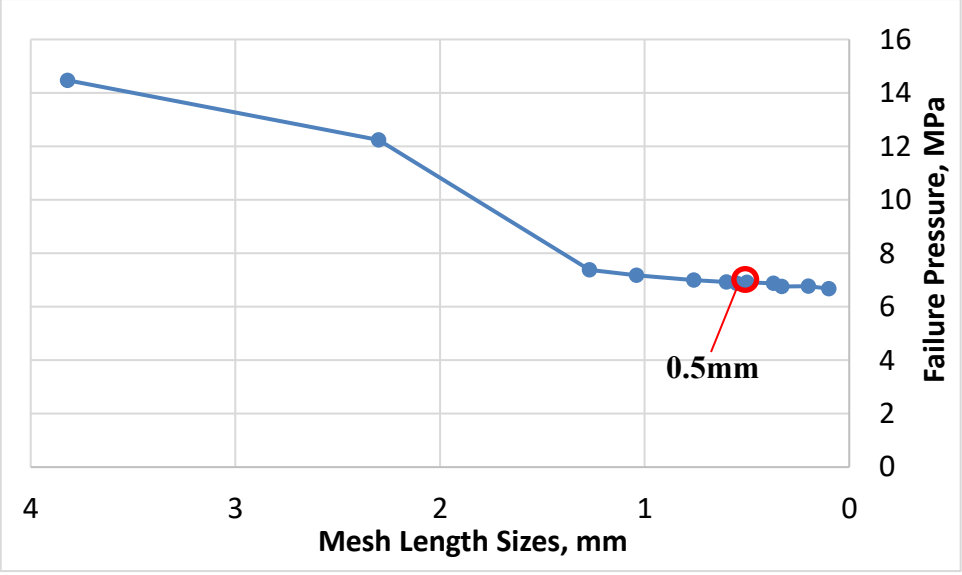

Figure 26: Failure pressure for different mesh length sizes for elastic-plastic material model.

Similarly, in Figure 26, it was observed that the failure pressure stabilized after l_h has reached a value of 0.5 mm. It was deduced that the failure pressure would stabilize when the mesh size was $l_h \times l_t$ = 0.5 mm × 0.67 mm. Therefore, this mesh size was chosen to investigate the effect of the CIC parameters on the failure pressure of the elastic-plastic model.

By comparing the results in the Figure 23-26, it can be seen that the elastic-only material model would yield a higher failure pressure than the elastic-plastic material model, and it would also require a finer mesh to achieve a stabilized failure pressure prediction. This could be attributed to the fact that the stress-strain curve for the elastic material is linear. Once the strain limit is reached, the material is expected to behave in a brittle manner because of the chosen low value of the fracture energy material parameter. However, for the elastic-plastic material, the material exhibits some plasticity before the crack propagates through the mesh which leads to a more ductile performance, such that a coarser mesh can be employed to achieve mesh convergence.

In the past, numerous researchers have studied mesh size sensitivity following both FEM and XFEM approaches. Munjiza et al. [65] investigated the mesh sensitivity by modelling a 2D fracture model using the combined FEM-based and Discrete Element Method (DEM)-based method. It was found that in order to accurately represent the bonding stress close to the crack tip, the elements size close to the crack tip should be much smaller than the length of the plastic zone ahead of the crack tip. Schwalbe et al. [66] proposed that the size of the element in the direction of crack propagation was recommended to be chosen in the range of 0.05 mm to 0.2 mm for ductile materials in FEM.

Lin et al. [59] simulated an X52 pipe steel in three dimensions and examined the numerical stability by changing the mesh size surrounding the crack propagation path, and it was demonstrated that even a much coarser mesh size of $l_h \times l_l \times l_t$ = 0.5 mm × 0.5 mm × 2 mm would be sufficient for XFEM simulation, in comparison to FEM modelling. They concluded that this mesh provided an optimal balance between computational speed and accuracy for predicting crack propagation in pipelines with various steel grades using XFEM. Similarly, Agbo et al. [67] conducted another mesh sensitivity analysis for 3D XFEM simulation, where three XFEM models with different mesh sizes (0.9mm, 0.45mm, and 0.3mm) aligned the crack propagation direction were simulated, considering a balance between computational cost and model accuracy, they concluded that a mesh size of 0.45 mm was optimal.

Although the previous investigation for mesh size sensitivity were focused on crack-only defects and our work is focusing on crack in corrosion defects, these mesh sizes are consistent with our findings for 2D XFEM simulations which concluded that the optimum mesh dimensions were $l_h \times l_t$ = 0.37 mm × 0.55 mm and $l_h \times l_t$ = 0.5 mm × 0.67 mm for elastic-only material model and elastic-plastic material model, respectively.

3.3.3 Effects of CIC Parameters on the Failure Pressure

1) Elastic-only Material Model

Depth of the Crack

Table 1 shows the variation of the failure pressure with increasing initial crack depth at constant total defect depth.

Table 1: Failure pressure for different initial crack depths (elastic model).

Depth of the Crack (mm)	d_{cr}/d_T	Failure Pressure (MPa)
0.5	0.1	23.78
1.25	0.25	21.3
2.5	0.5	14.81
3.75	0.75	14.59
5	1	14.75

At $d_{cr}/d_T = 0.1$, the failure pressure is the highest at 23.78 MPa, but when d_{cr}/d_T was increased to 0.5, the failure pressure fell significantly to 14.8 MPa. The failure pressure continued to drop gradually to 14.59 MPa, as d_{cr}/d_T increased. The failure pressure increased slightly to 14.75 MPa at $d_{cr}/d_T = 1$.

The differences in the predictions of failure pressure between the last two models is minimal, and it can be inferred that increasing the crack beyond a critical value of around 50% of the total defect may not lead to substantial changes in the failure pressure.

Width of the corroded area

Table 2 shows the variation of the failure pressure with increasing corroded area width at constant total defect depth, d_T.

Table 2: Failure pressure for different corrosion widths (elastic model).

Width of Corroded Area (mm)	Failure Pressure (MPa)
10	14.81
15	14.6
20	14.73

A slight decrease in the failure pressure was observed, and the result illustrates that the width of the corroded area only has little impact on the failure pressure.

Corrosion Profile

Table 3 shows the variation of the failure pressure with different corrosion profiles.

Table 3: Failure pressure for different corrosion profiles (elastic model).

Corrosion Profile	Failure Pressure (MPa)
Semi-elliptical	14.81
Semi-rectangular	14.36

It was observed that the failure pressure of the model with a semi-elliptical corrosion profile is slightly higher than that with a semi-rectangular profile, so the influence of the corrosion profile on the failure pressure can be considered negligible.

2) Elastic-plastic Material Model

Depth of the Crack

Table 4 shows the variation of the failure pressure with increasing crack depth at constant total defect depth.

Table 4: Failure pressure for different initial crack depths (elastic-plastic model).

Depth of the Crack (mm)	d_{cr}/d_T	Failure Pressure (MPa)
0.5	0.1	7.64
1.25	0.25	7.34
2.5	0.5	6.91
3.75	0.75	6.32
5	1	6.27

At $d_{cr}/d_T = 0.1$, the failure pressure is the highest at 7.647 MPa, but when d_{cr}/d_T was increased to 0.5, the failure pressure fell slightly to 6.915 MPa. The failure pressure continued to drop to 5.76 MPa. The result showed that failure pressure decreased with increasing crack depth. Unlike the elastic model, which exhibited a stabilization of the failure pressure beyond a critical value for the crack depth, the failure pressure for the elastic-plastic model continued decreasing with the increase of the crack depth.

Ma et al. [20] studied the influence of crack depth on the failure pressure using traditional FEM simulations in 3D. Only one quarter of the pipe was modeled, and ten FE models were built. Two failure mechanisms were applied (i.e., crack growth and plastic collapse), and the final failure pressure was the least of the two failure pressure values. The failure pressure against crack depths for two toughness levels were plotted. Both curves showed that the failure pressure first decreased

slightly with increasing d_{cr}/d_T; the failure pressure kept decreasing until $d_{cr}/d_T = 0.5$, and it began to increase as d_{cr}/d_T increased beyond 0.5. Their results are different from our model predictions, which exhibited a continually decreasing trend of the failure pressure with increasing crack depth. The differences in the results could be attributed to the fact that the ratio of the pipe outside diameter to pipe thickness was different. In addition, our models are simply 2D while Ma et al. [20] modeled their pipes in 3D.

Mondal et al. [68] simulated five FE models in 3D where the failure pressure for CIC defects was determined based on two different approaches (von Mises criterion and fracture criterion); Initially, the failure pressures calculated using several models (including the modified ASME B31G, DNV-RP-F101, and a model recently proposed by Mondal and Dhar [69]) were compared with the failure pressure predicted using FE analysis to examine the effectiveness of the model in predicting the failure pressure of pipelines with corrosion-only defect. The result shows that the failure pressures calculated using the models proposed by Mondal and Dhar [69] are less conservative among different models.

In order to investigate the effect of initial crack depth on the burst pressure of pipelines with CIC defect, during the analysis, the initial crack depth was varied (ranging from 0.5 mm to 2 mm) while the crack length (l_c), corrosion depth (d) and corrosion length (l) were kept constant. The failure pressure for CIC defects was normalized by the failure pressure of pipelines with corrosion-only defect, the crack depths were normalized by the wall thickness. The failure pressure for corrosion-only defect (P_f) was calculated using the equation proposed in Mondal and Dhar [69]:

$$P_f = \frac{2t}{(D-2t)}\sigma_{UTS}\left\{\frac{1-\frac{d}{t}}{1-\frac{d}{tM_t}}\right\} \quad (26)$$

where,

$$M_t = \sqrt{1 + 0.278\left(\frac{l^2}{Dt}\right)^{0.447} \times \left(\frac{d}{t}\right)^{-0.718} + 0.337\left(\frac{l^4}{D^2t^2}\right)^{0.717} \times \left(\frac{d^2}{t^2}\right)^{0.504}} \quad (27)$$

Mondal et al. [68] employed D = 508 mm, t = 5.7 mm, d = 2.0155 mm, l = 200 mm and σ_{UTS} = 631 MPa.

The normalized failure pressures (P/P_f) against normalized crack depths (d_{cr}/t) were plotted. The result showed that the von Mises criterion provided higher failure pressure than the fracture criterion and the burst pressure decreased nonlinearly with the increase of the crack depth for both approaches. More specifically, the differences between the last three models were minimal, supporting the conclusion that a stabilization exhibited in the burst pressure when the ratio of the crack depth to the wall thickness reached a critical value of around 0.25. Unlike our elastic-plastic model, the failure pressure continued decreasing with the increase of the crack depth.

An artificial corrosion-only model with semi-elliptical profile was constructed in ABAQUS and the failure pressure was predicted using XFEM. The total defect depth remained 5 mm, while the width of the corrosion area and the corrosion depth were set as 10 mm and 5 mm, respectively. The failure pressure against different d_{cr}/d_T (ranging from 0 to 1) was plotted below.

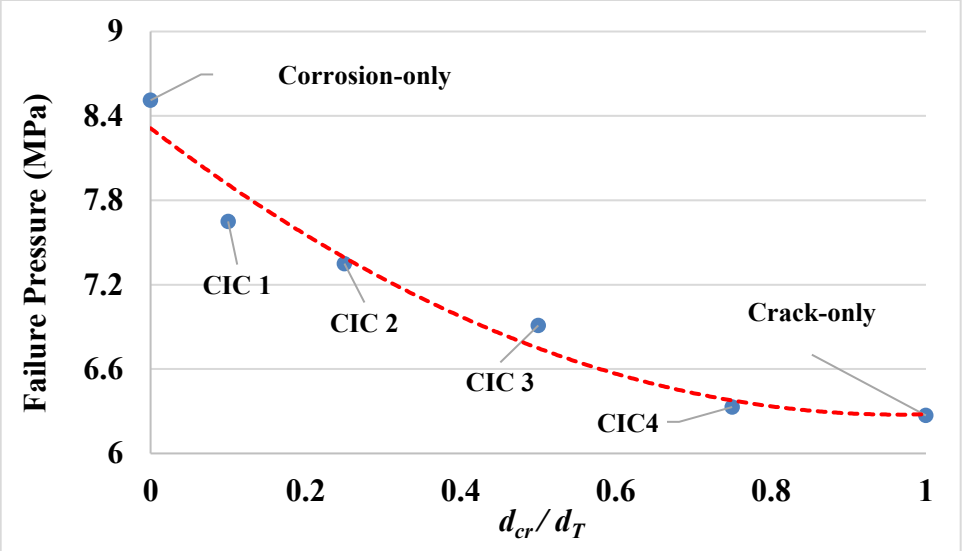

Figure 27: Failure pressure for different CIC defects with varying crack & corrosion ratio (when the total defect depth = 50%WT).

As shown in Figure 27, the crack-only defect is more critical than the corrosion-only defect of equivalent depth and the failure pressure for a CIC defect varied between a crack-only defect and a corrosion-only defect. More specifically, the failure pressure seems to stabilize for the two models with d_{cr}/d_T = 0.75 and 1 implying that for CIC defects having a crack that is bigger than 50% of the total depth of the defect could be treated as a crack-only defect with the total depth of the defect being the crack depth.

Width of the corroded area

Table 5 shows the variation of the failure pressure with increasing corroded area width at constant total defect depth, d_T.

Table 5: Failure pressure for different corrosion widths (elastic-plastic model).

Width of Corroded Area (mm)	Failure Pressure (MPa)
10	6.91
15	6.9
20	6.85

A slight decrease in the failure pressure was observed, and the result illustrates that the width of the corroded area has little impact on the failure pressure.

Ma et al. [20] investigated the influence of the width of the corrosion area on the failure pressure by simulating several FE models at two different d_c/d_T ratios (d_c/d_T = 0.5 and 0.92). During the 3D simulation, the corroded area width ranged from 25.4 mm to 431.8 mm, while the lengths of the crack and the corrosion area were fixed at 101.6 mm and 152.4 mm, respectively. The failure pressure against corrosion area widths at two d_c/d_T ratios were plotted. Both curves were flat over most of the part of the width range with the failure pressure remained at around 8.27 MPa and 9.65 MPa, respectively. They concluded that the width of the corroded area only has a secondary impact on the failure pressure, and that inference is in agreement with our findings.

Corrosion Profile

Table 6 shows the failure pressure with two different corrosion profiles of equivalent depths.

Table 6: Failure pressure for different corrosion profiles (elastic-plastic model).

Corrosion Profile	Failure Pressure (MPa)
Semi-elliptical	6.91
Semi-rectangular	6.84

It was observed that the failure pressure corresponding to the semi-elliptical corrosion profile is slightly higher than that with a semi-rectangular profile, this difference could be attributed to the difference in the total void space associated with these two geometries: more material was removed in the semi-rectangular profile; the situation was further exacerbated by abrupt changes in at the corners and that might lead to locally-concentrated stress distribution and overall higher stresses across the corrosion area. The result illustrates that the corrosion defect in the circumferential direction has little effect on the failure pressure.

The same conclusion was obtained by Han et al. [6] who built five 3D FE models of pipelines with corrosion-only defects. The aim of their study was to investigate the effect of circumferential width of the corrosion area on the failure pressure. The failure was predicted to occur at the corroded pipeline when the minimum von Mises stress was greater than the tensile strength. The failure pressures of the corroded pipeline calculated using different methods (ASME B13G-2009 [70] and FEA) were compared and the result shows that the failure pressures with varying corrosion depths were almost the same. In order to obtain more accurate results, ASME B13G-2009 method was selected to predict the failure pressure, using the equation that has been mentioned earlier. It was

observed that there was little variation in the failure pressure associated with the changes in the corroded area width and they concluded that the circumferential width of the corroded defect had a very small effect on failure pressure.

CHAPTER 4: XFEM PARAMETER CALIBRATION AND MODEL VALIDATION[2]

4.1 Introduction

The objective of Chapter 4 is to create a set of validated numerical finite element analysis models that are suitable for accurately predicting the failure pressure of 3D cracks-in-corrosion defects using the XFEM technique. Five burst tests of API 5L X60 specimens with different defect depths (varying from 52% to 66%) that are available in the literature [13] were used to calibrate the XFEM damage parameters (the maximum principal strain and the fracture energy). These parameters were varied until a reasonable match between the numerical results and the experimental measurements was achieved. A longitudinally oriented CIC defect was placed at the exterior of the pipe. The profile of the corroded area was assumed to be semi-elliptical. The pressure was monotonically increased in the XFEM model until the crack or damage reached the inner surface of the pipe. Six more CIC models with the same pipe dimension but different crack depths were constructed to investigate the relationship between the initial crack depth and the failure pressure. The versatility of RSTRENG, LPC, and CorLAS in predicting the failure pressure was also examined by comparing the results with the XFEM predictions.

[2] A version of this chapter has been published in the conference proceedings:

Zhang, X.F., Okodi, A., Tan, L.C., Leung, J.Y., and Adeeb, S. Forthcoming. Failure pressure prediction of crack in corrosion defects using XFEM", IPC 2020-9312, Proceedings of the 18th Internal Pipeline Conference, Calgary, Canada, 2020.

4.2 Methodology

Dimensions of the pipe and defects were all extracted from Bedairi et al. [13]. More specifically, the outer diameter of the pipe (D) was taken as 508 mm with 5.7 mm wall thickness (t). The crack was 100 mm in length, while the corrosion defect length (l) and width were assigned constant values of 200 mm and 30 mm, respectively. In general, an XFEM crack is simulated as a planar crack inserted into the pipe model; however, our initial models indicated that using a planar crack generated initial crack cohesion and resistance near the crack tip field which led to inaccurate predictions. Furthermore, modeling a physical crack instead of a planar crack in the model could provide more accurate results. Mondal et al. [68] examined the effects of a V-notch shaped crack and a blunt-tip crack on the J-integrals and the failure pressure. The results showed that the two shapes of cracks leading to similar failure pressures with a difference of approximately 9%. To account for simplicity in modelling, a V-notch shaped crack was suggested [68]. In this study, the CIC defect was generated at the outer surface of the pipe, where the crack was simulated as a V-notch shaped crack and the corrosion region was simulated as a semi-ellipsoid. The length of the pipe model was selected as 3000 mm which is greater than the minimum length that was recommended in Fekete et al. [71]. The equation can be expressed as follows:

$$L_{min} = \frac{l}{2} + \frac{d}{t}\sqrt{Dtl} \tag{28}$$

In the analysis, the geometric non-linearity option was chosen. In order to improve the model accuracy, the initial and the maximum increment size were set as 0.005, the minimum increment size was set as 1e-15, and the maximum number of allowable increments was 1000.

The boundary conditions were chosen to allow for pipe expansion due to variation in the internal pressure. In order to reduce the computational efforts and take the advantage of symmetry, only half of the full pipe was modelled, as shown in Figure 28. The remote end of the model was symmetrically restricted in the Z-direction. Kinematic coupling constraint was applied at the location of the fixed boundary condition allowing the pipe to expand but stay on the same plane.

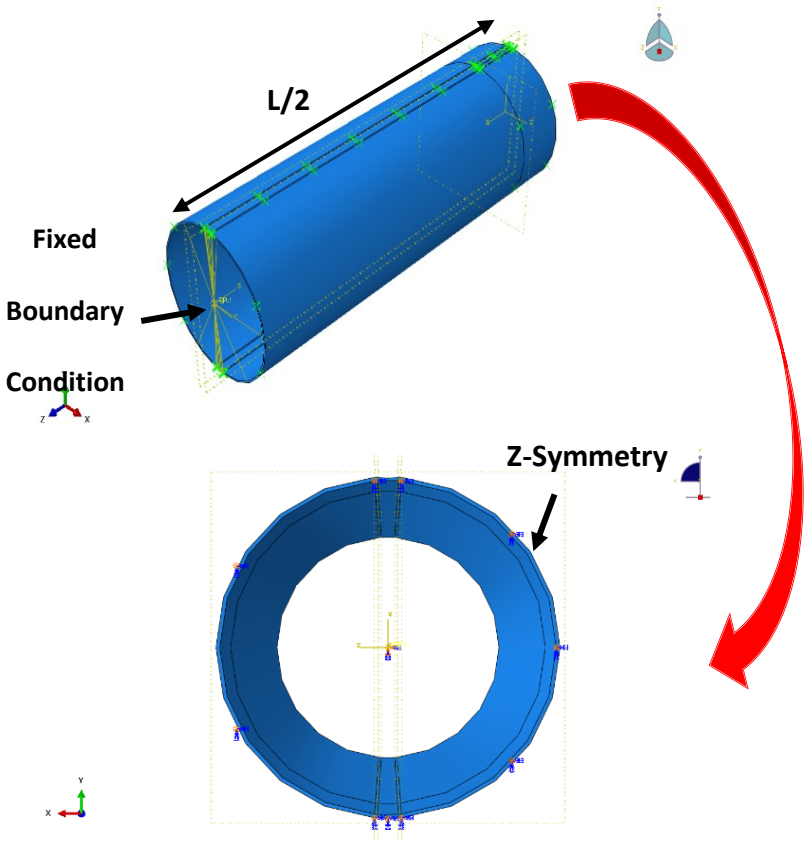

Figure 28: The finite element model geometry showing the boundary conditions and loading.

4.3 Material Properties

The XFEM was performed using the commercially available software package, ABAQUS Version 6.19 [19]. The pipe was assumed to be composed of an elastic-plastic isotropic material, with modulus of Elasticity (E) and the Poisson's ratio (υ) of 207 GPa and 0.3, respectively. The following values were assigned to initialize the XFEM parameters: The maximum principal strain damage initiation tolerance was set as 0.5; ABAQUS also requires the input of a viscosity coefficient, and the recommended default value of 1e-5 was used. The true circumferential stress-strain data were obtained using the Ramberg-Osgood equation [13].

$$\epsilon = \frac{\sigma}{E} + \alpha \left(\frac{\sigma}{\sigma_{YS}}\right)^{n-1} \left(\frac{\sigma}{E}\right) \tag{29}$$

Bedairi et al. [13] employed these values: σ_{YS} = 435 MPa, α =1.75 and n = 9.35. The true stress-strain curve obtained using Eq. (29) is shown in Figure 29.

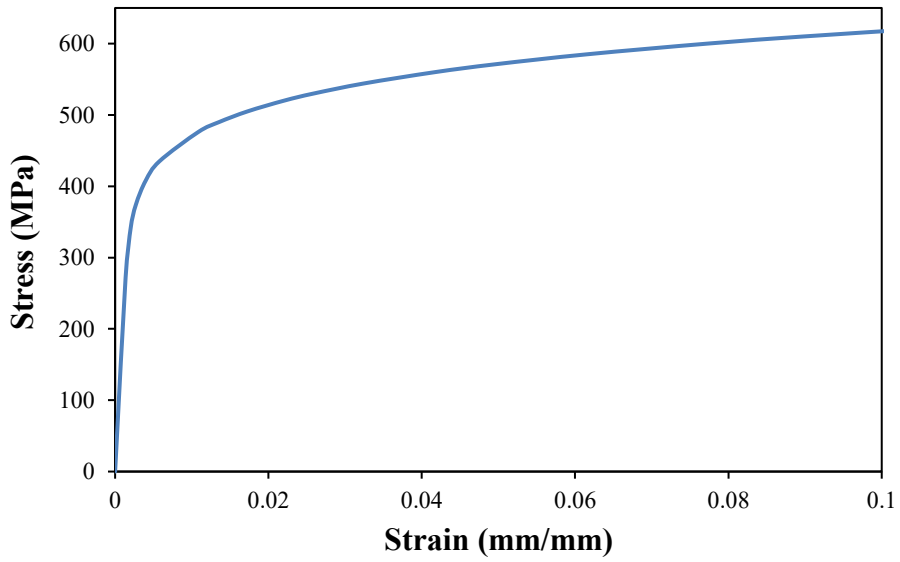

Figure 29: True stress-strain curve of pipe steel (X60), adopted from Bedairi et al. [13].

4.4 Model Validation

4.4.1 Calibration of XFEM Parameters

The use of either the maximum principal strain (M_{axpe}) or the maximum principal stress (M_{axps}) as the damage parameter was investigated by Okodi and Agbo [47,67]. It was reported that the models using M_{axpe} could replicate the failure pressure of full-scale tests of pressurized cracked pipelines using one set of damage parameters, whereas M_{axps} failed to do so. Therefore, M_{axpe} and fracture energy (G_c) were selected in the current study as the adjustable XFEM damage parameters.

During the validation process, these two key XFEM damage parameters were calibrated using the full-scale test data obtained from [13]. Initially, the maximum principal strain was set as 0.005; damage evolution was controlled by the fracture energy which was set as 10 N/mm. During the analysis, in order to determine the optimal set of damage parameter, the two values were varied until the failure pressures obtained from the XFEM numerical study matched well with those obtained from the rupture tests. The optimum prediction was achieved when the damage parameters were set as $M_{axpe} = 0.02$ and $G_c = 150$ N/mm; thus, this damage parameter set was used for subsequent analyses. It is interesting to note that the value obtained for G_c is slightly less than half the value of the fracture energy derived from Charpy V-Notch (CVN) testing requirements of API 5L X60 steel (27J minimum): 27J/10^8 mm^2 = 327.5 N/mm [21]. The G_c XFEM parameter is a measure of the area under the curve of the descending branch of the force displacement curve of a material after reaching its peak load and is expected to be smaller than the total fracture energy derived from CVN.

4.4.2 Mesh Details

The mesh size must be chosen to satisfy the balance between computational time and the accuracy of the results. In order to ensure calculation accuracy, we modelled the defect region with a fine mesh that increased in size away from the cracked region. In our previous work [3], the mesh size sensitivity investigation was conducted in 2D for determining the optimal mesh size and it was concluded that for ductile material, the element size in the circumferential direction (l_h) and thickness direction (l_t) of 0.5 mm × 0.67 mm was sufficient to predict the failure pressure for crack in corrosion defects. Since the pipe diameter and wall thickness were different in [3], for the current study in 3D, mesh size sensitivity was conducted by running the XFEM model with three different mesh sizes (0.8 mm, 0.5 mm, and 0.25 mm) along the crack propagation direction. The results indicated that the mesh size of 0.8 mm gives a conservative result at the best computational time while the mesh size of 0.5 mm gives a more accurate result at a good computational time, but the mesh size of 0.25 mm leads to almost the same result with 0.5 mm at a more expensive computational cost. Therefore, the element size of 0.5 mm × 0.5 mm along the l_h, l_t directions were used in this paper. The same values of mesh sizes were used by Lin et al. [59]. Partitions were created in order to control the generated mesh for different regions around the crack as shown in Figure 30.

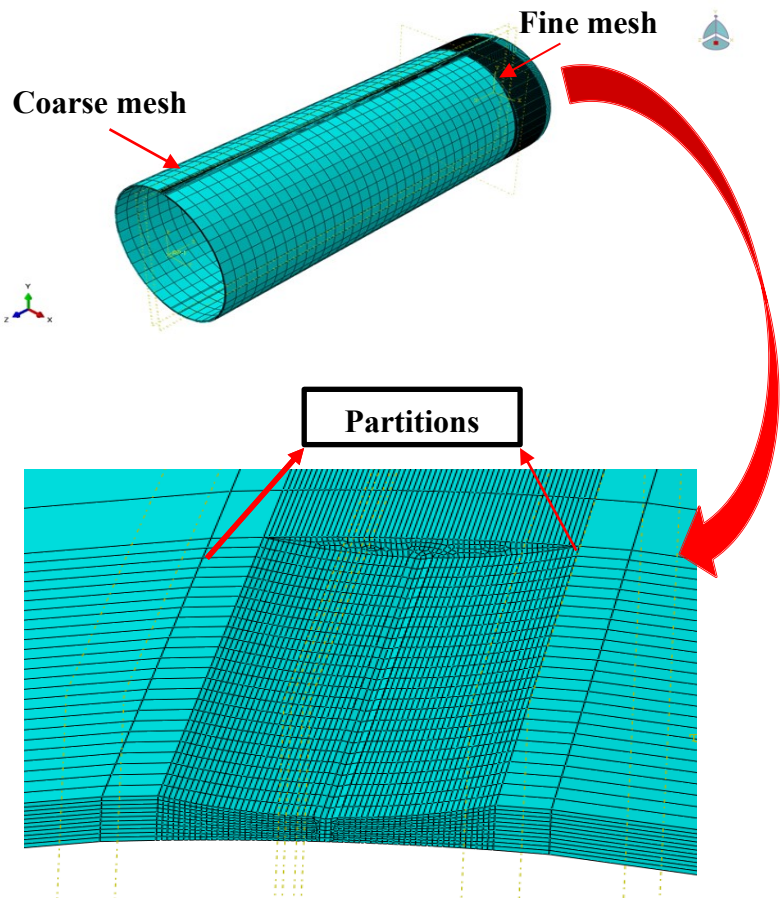

Figure 30: A typical XFEM mesh.

4.5 Numerical Analysis

4.5.1 Cracks in corrosion (CIC) Defect

Each CIC defect was modelled as a corrosion defect with an elliptical profile and a crack. A pre-defined location of the crack was considered. In the current study, a notch was created at the center of the corrosion to represent the crack. The total defect depth is defined as the combined depth of the crack depth and corrosion depth, as a percentage of the wall thickness (t).

Several XFEM models were developed using the dimensions of the CIC defects reported in [13] and they are summarized in Table 7. The failure criterion was satisfied when the crack reached the last element, and the corresponding pressure was recorded as the failure pressure.

Table 7: CIC defects geometry [13].

Test ID	Corrosion & Crack Length (mm)	Corrosion Width (mm)	Defect Depth		Total Defect Depth (%WT)
			Crack (%WT)	Corrosion (%WT)	
CIC 1	200	30	16.6	35.4	52
CIC 2			22.4	36.6	59
CIC 3			20.4	39.6	60
CIC 4			18.3	42.7	61
CIC 5			23.1	42.9	66

4.5.2 Effect of d_{cr}/d_T

In order to examine the effect of crack depth on the failure pressure of a pipeline containing CIC defects, six more CIC models with the same pipe dimensions but varying initial crack depths were analyzed on the outer surface of the pipe sections (the d_{cr}/d_T ratio was varying from 0 to 1). The corrosion defect was 200 mm in length and 30 mm in width (a typical artificial corrosion profile was shown in Figure 31) whereas the crack defect length was 100 mm. The total defect depth in this part of the analysis was fixed at 50%WT. Later, the versatility of the RSTRENG, LPC, and CorLAS methods in predicting the failure pressure was examined by comparing with the numerical results.

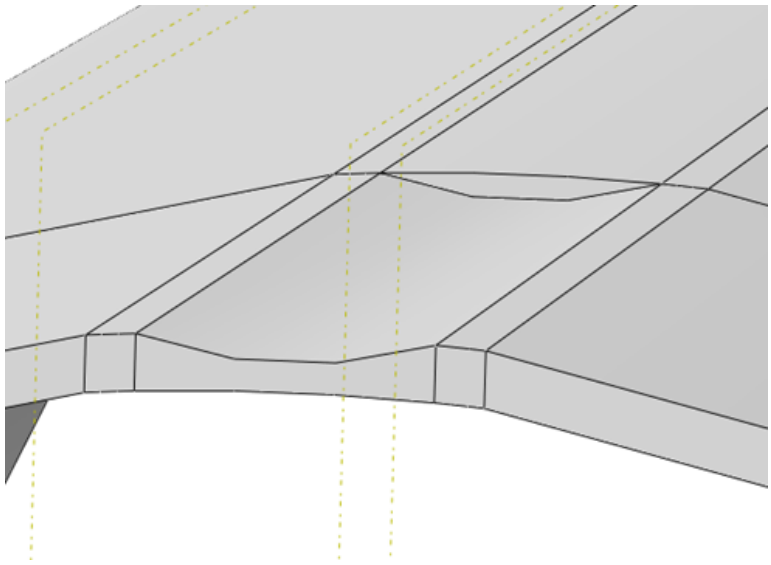

Figure 31: The profile of an artificial corrosion defect.

4.6 Results & Discussion

4.6.1 CIC Defects Results & Evaluation

Table 8: Comparison between experimental and XFEM results for CIC modelling.

Test ID	Total defect depth (%WT)	Experimental failure pressure (MPa)	XFEM predicted failure pressure (MPa)	Difference (%) between experimental and predicted failure pressure
CIC1	52	7.74	8.11	- 4.78
CIC2	59	6.72	7.4	-10.1
CIC3	60	7.06	7.14	-1.13
CIC4	61	7.89	6.9	12.54
CIC5	66	6.15	6.3	-2.4
			Average	5.87

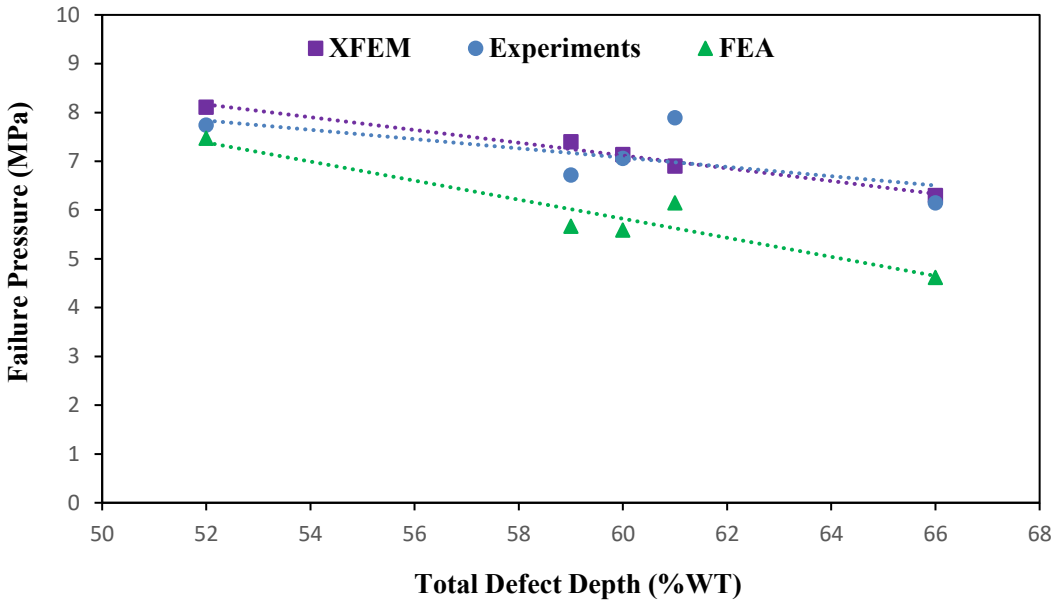

Figure 32: Comparison between XFEM, experimental, and FEA results for CIC modelling. FEA and experimental results were reported by Bedairi et al. [13].

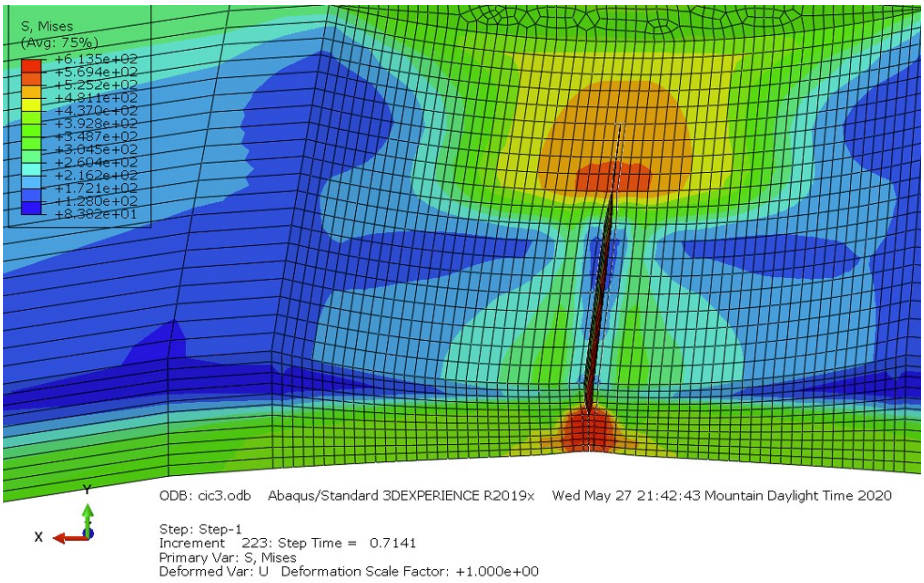

Figure 33: 60%WT CIC defect model.

The predicted failure pressures obtained from XFEM were compared with the rupture test data of Bedairi et al. [13] and the results are shown in Table 8 and Figure 32. Figure 33 shows a typical CIC defect model (60%WT) subjected to internal pressure of 10 MPa.

As shown in Figure 32, the failure pressure computed using the FEA models, as reported by [13] did not match well with the experimental results, with deviations of 3.49%, 15.7%, 20.9%, 22%, and 24.8%, respectively. The FEA models consistently underestimated the failure pressure, and the discrepancy increased with the increase in total defect depth. On the other hand, the XFEM prediction results obtained from the current study (Table 8) matched closely with the experimental data obtained from [13], with an average error of 5.87%, which was less conservative than the FEA method, with an average error of 17.4%. The difference could be attributed to the fact that Bedairi et al. [13] used the J-integral based fracture criterion to evaluate the failure pressure. More specifically, when the J-integral value reached $J_{0.2}$, the model was considered to fail by fracture. While in this paper, the failure was simply defined as the moment when the damage reached the last element.

4.6.2 Effect of d_{cr}/d_T Results & Evaluation

To examine the effect of d_{cr}/d_T on the failure pressure, the failure pressures corresponding to different d_{cr}/d_T ratios, while the total defect depth was 50%WT. Six XFEM models were constructed, and the results are plotted in Figure 34. For example, when the crack depth is 0%, the corrosion depth is 50%, when the crack depth is 25%, the corrosion depth is 25%.

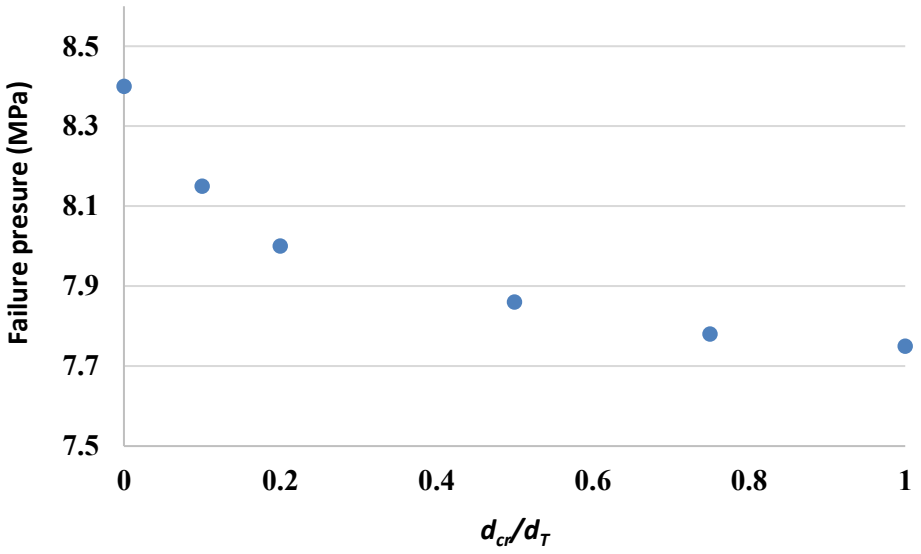

Figure 34: Failure pressure for different CIC defects in 3D with varying d_{cr}/d_T ratio when the total defect depth = 50%WT. (Results based on X60 pipe material)

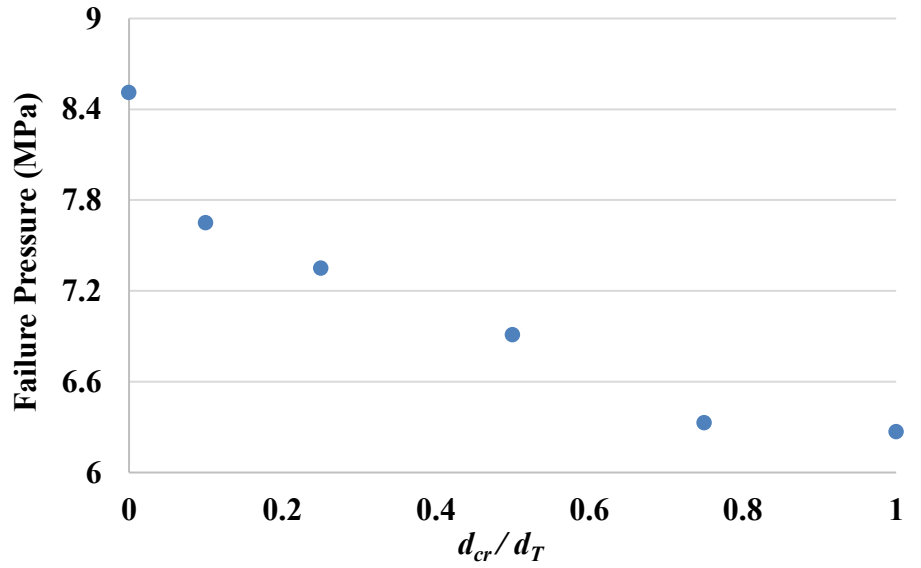

Figure 35: Failure pressure for different CIC defects in 2D with varying d_{cr}/d_T ratio (when the total defect depth = 50%WT), adopted from [3].

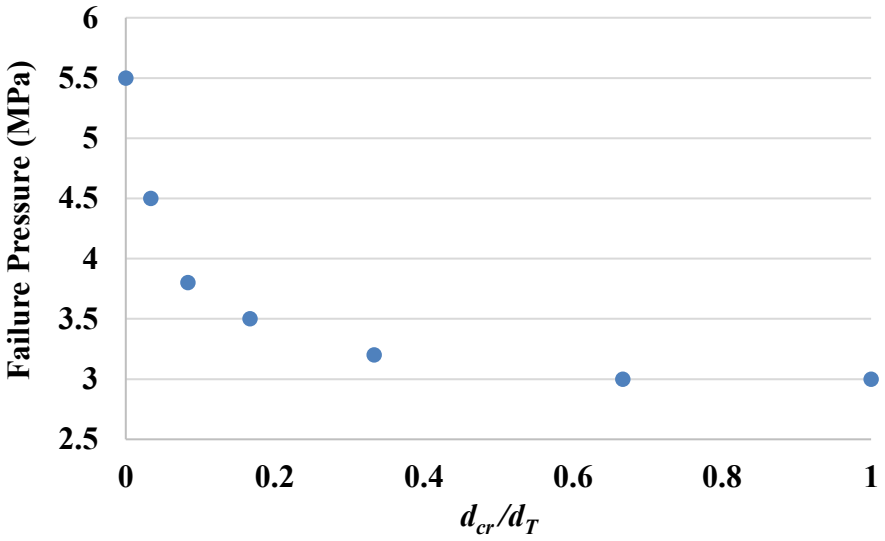

Figure 36: Predicted failure pressure for CIC defects in 3D with varying d_{cr}/d_T ratio, the total defect depth = 60%WT, adopted from [64]. (Results based on X52 pipe material)

As expected, the corrosion-only defect exhibited a higher failure pressure than the crack-only defect, and the predicted failure pressures decreased non-linearly with the increase in crack depth, as shown in Figure 34. When $d_{cr}/d_T = 0$, the failure pressure was determined using the corrosion-only model, and its value was the highest. When $d_{cr}/d_T = 1$, the failure pressure was the lowest, and it was determined by the crack-only model. It is observed that the predicted failure pressures for the CIC model would approach that for the crack-only model when $d_{cr}/d_T = 0.75$ and 1; therefore, it can be inferred that increasing the initial crack depth beyond a critical value of approximately 50% of the total defect depth may not lead to substantial changes in the failure pressure. To summarize, a CIC defect could be treated as a crack-only defect when the initial crack depth exceeded 50% of the total defect depth.

A parametric study was conducted in our previous work [3] in 2D in order to investigate the effect of different CIC parameters on the failure pressure. Five CIC defects with different initial crack depths (ranging from 0.5 mm to 5 mm) were evaluated. It was found that the initial crack depth had a significant effect on the failure pressure as opposed to the width of corroded area and corrosion profile which have only a negligible effect on the failure pressure. The predicted failure pressures against the d_{cr}/d_T ratio in 2D was shown in Figure 35, the failure pressure for a CIC defect was found to vary between that of a crack-only defect and a corrosion-only defect. Moreover, a CIC defect could be treated as a crack-only defect to evaluate the failure pressure when d_{cr}/d_T ratio exceeded 0.5, since the failure pressure predicted using the CIC or crack-only models would yield similar values for d_{cr}/d_T = 0.75 and 1. It is shown that a similar decreasing trend of failure pressure versus d_{cr}/d_T was also observed in the 3D cases, despite the difference in the pipe geometry and material properties.

The findings of this study are also corroborated by Cronin et al. [64] who investigated the effect of corrosion depth on the failure pressure by constructing five FE models with various crack and corrosion depths, for a constant total defect depth of 60%WT. The FE models were designed as a uniform depth and circular shape at the crack ends. The dimensions of the pipe were taken from their previous study where the outer diameter and the pipe wall thickness were 864 mm and 9.53 mm, respectively. The failure pressures for crack-only defects and corrosion-only defects were investigated separately in order to evaluate the CIC behavior. Failure was predicted to occur when the J-integral value exceeded the critical value ($J_{0.2} = 120\ \mathrm{kJ/m^2}$). Figure 36 shows the predicted failure pressure for the CIC defects as a function of d_{cr}/d_T ratio. It is apparent that the predicted failure pressures decreased with the increase of d_{cr}/d_T ratio. They also concluded that the failure

pressure would converge towards that of the crack-only defect when the crack depth approached the total defect depth, a trend that is consistent with our conclusion.

It should be noted that in the model where the d_{cr}/d_T ratio in Figure 34 is 0, representing a corrosion-only defect, and since the crack location was unknown, XFEM was used here to identify the crack location. As mentioned earlier, a comparison between the XFEM predictions, RSTRENG, LPC, and CorLAS predicted results were conducted to investigate the effectiveness of each method in predicting the failure pressure for pipelines with different defects (Table 9 and 10). CorLAS (Version 2.0) was used here, since CorLAS (Version 1.0) was found to be conservative for long cracks [72].

Table 9: Comparison between XFEM, RSTRENG, and LPC for corrosion modelling.

Model ID	Predicted failure pressure (MPa)			Difference (%)	
	XFEM	RSTRENG	LPC	RSTRENG	LPC
C1	8.4	6.8	8.7	19	3.5

Table 10: Comparison between XFEM, and CorLAS (Version 2.0) for crack modelling.

Model ID	Predicted failure pressure (MPa)		Difference (%)
	XFEM	CorLAS	
CR1	7.75	7.2	7

Table 9 shows that the predicted failure pressure for the corrosion-only scenario was closer to the one calculated using the LPC method than RSTRENG method; The differences reported were 3.5% for the LPC method in comparison to 19% for the RSTRENG method. For the crack-only

defect, CorLAS method provided an estimate that is only 7% different from the one calculated using XFEM (Table 10).

CHAPTER 5: NUMERICAL MODELLING OF CIC DEFECTS IN API 5L X42 AND X52 LINEPIPES[3]

5.1 Introduction

The primary objective in this chapter is to provide general guidelines for assessing CIC defects in pipelines. The calibrated model from Chapter 4 with M_{axpe} = 0.02 mm/mm and G_c = 150 N/mm was used to predict the failure pressure for two sets of burst test data obtained from Ma et al. [20]. In their work, several full-scale burst tests were conducted on API 5L X42 and X52 vintage pipes. Each test was modeled using the extended finite element method and the experimental results were compared with the numerical predictions to validate XFEM models. A CIC defect was created at the outer surface of the pipe, where a V-notch shaped crack and a corrosion defect with elliptical profile were considered. Same fracture criterion as Chapter 4 was used. Later, the effect of initial crack depth on the failure pressure with various defect geometries was examined using both X42 and X52 materials.

5.2 Methodology

5.2.1 Numerical Model Set Up

Both API 5L X42 and X52 line pipes subjected to internal pressure were modelled in this study using the commercially available numerical software, ABAQUS v 6.19 [19], and the dimensions of the pipes and defects were all extracted from Ma et al. [20] and summarized in Table 11. The geometry configuration of the model is shown in Figure 37. The pipe geometry was modelled as a three-dimensional (3D) solid structure. Symmetry was used to reduce the size of the XFEM model

[3] A version of this chapter has been submitted to the International Journal of Pressure Vessels and Piping (IPVP).

and computer processing times; thereby only half of the full pipe containing the CIC defects was modelled, with a mesh size of $l_h \times l_l \times l_t$ = 0.5 mm × 0.5 mm × 5 mm, which is determined based on the results of mesh size sensitivity that conducted in Chapter 4. The lengths of the pipe models were selected in a way that the applied boundary conditions do not have an influence on the failure pressures [68]. Same boundary conditions as mentioned in Chapter 4 were applied to the model. The lengths of the pipe models were selected in a way that the applied boundary conditions do not have an influence on the failure pressures [68]. The CIC defect was generated at the outer surface of the pipe, where the crack was simulated as a V-notch shaped crack and the corrosion region was simulated as a semi-ellipsoid.

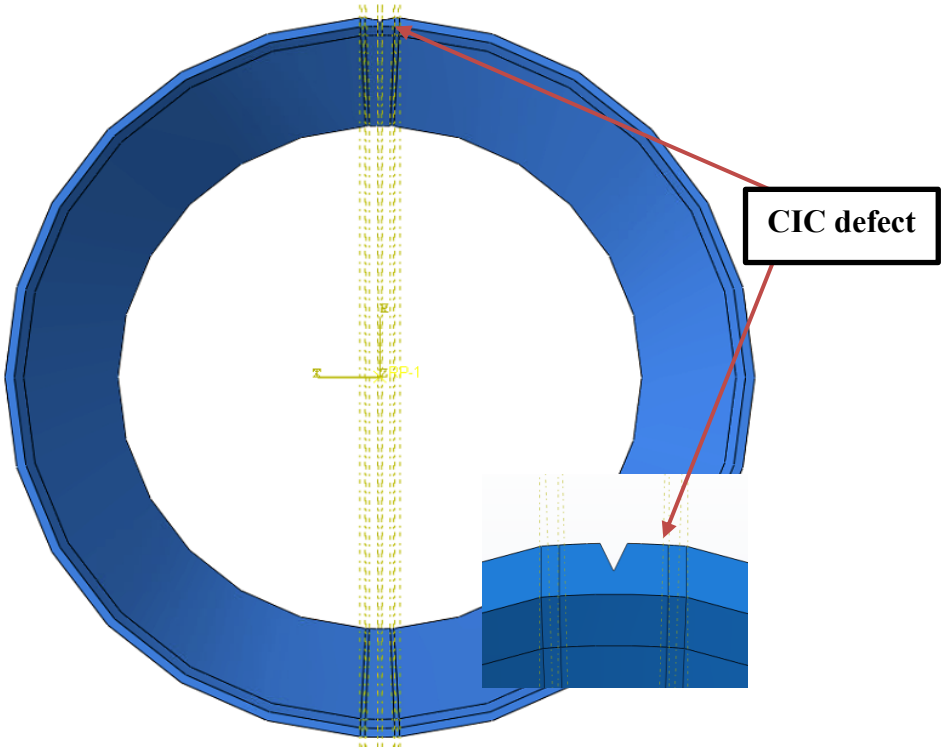

Figure 37: Schematic diagram of a CIC defect.

Table 11: Geometry of pipes [20].

Geometries (X42)	**Values**
Outside diameter, mm	273
Wall thickness, mm	6.35
Manufacture year	1958
Geometries (X52)	**Values**
Outside diameter, mm	762
Wall thickness, mm	9.52
Manufacture year	1952

5.2.2 Material Properties

The true stress-strain data were obtained from Ma et al. [20] using the Ramberg-Osgood equation (Eq. (23)). The X42 and X52 materials had Young's modulus E = 200 GPa, and Poisson's ratio ν = 0.3. The material properties were outlined in Table 12 and the stress-strain curves were shown in Figure 38.

Table 12: Material properties of X42 and X52 pipes [20].

X42 grade		X52 grade	
σ_{YS}	σ_u	σ_{YS}	σ_u
342	411	363	484

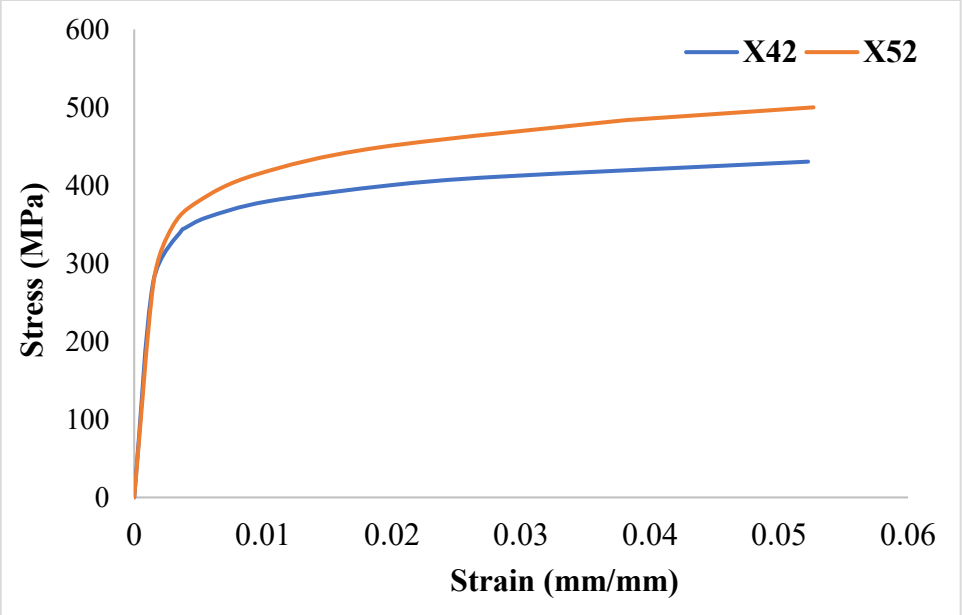

Figure 38: Stress-strain curves constructed from Ramberg-Osgood equation [20].

5.3 X42 Grade Results & Discussion

5.3.1 Model Validation

In our previous study [73], the maximum principal strain, M_{axpe}, and the fracture energy, G_c were selected as the damage parameters. M_{axpe}, determines the initiation of the fracture, whereas G_c, controls the crack growth rate. The damage parameters were calibrated using the burst test results from Bedairi et al. [13] and it was found that the predictions were reasonably accurate for all of the burst tests when the damage parameters were M_{axpe} = 0.02 mm/mm and G_c = 150 N/mm. Therefore, in this work, the calibrated model was used to predict the failure pressure.

The XFEM model was initially validated using the results from Ma et al. [20]. The specimens were cut out from a 10.75-inch OD and 0.25-inch WT API 5L X42 line pipe that contained CIC defects. The corrosion defects, 152.4 mm long, 50.8 mm wide, were machined on the outer surface of the pipe with different depths (70%, and 90% of d_T), while the total defect depth was 60%WT. Each

CIC defect was modelled as a corrosion defect with an elliptical profile and a V-notch shaped crack. The predicted XFEM failure pressures were compared with the FEA predictions [20] and the experimental results obtained from [20], as shown in Figure 39.

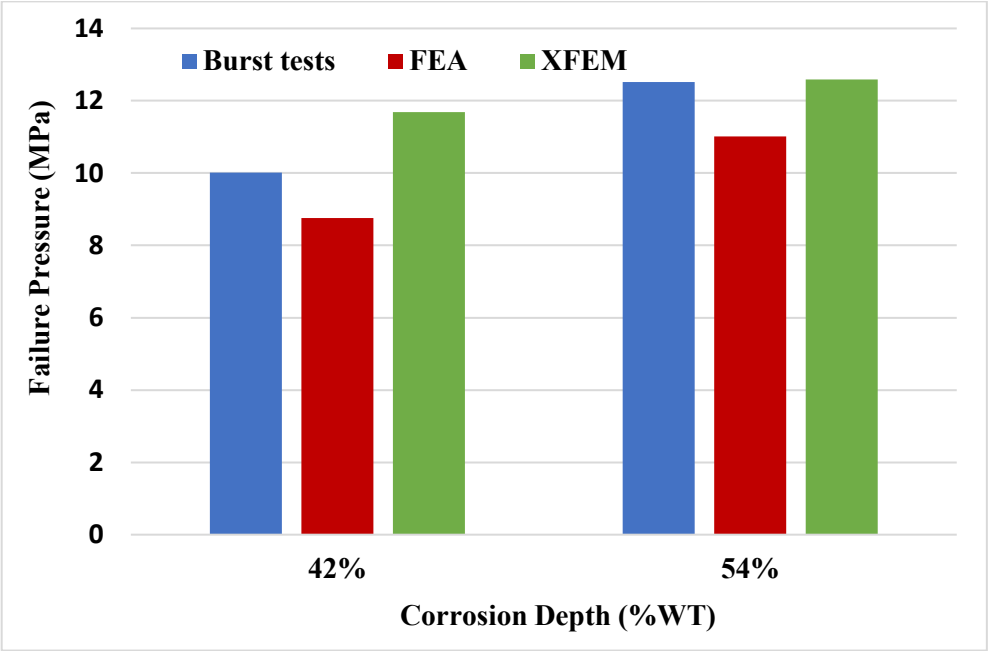

Figure 39: Comparison between XFEM, experimental, and FEA results for CIC modelling. FEA and experimental results were reported by Ma et al. [20].

The difference between the experimental, FEA, and XFEM results can be seen from Figure 39. It is noted that when the ratio of corrosion depth to wall thickness was 0.42, neither the XFEM nor FEA predictions agreed well with the experimental data, with an error of approximately 12%. However, the XFEM predictions aligned with the burst test data when the corrosion depth was 54 %WT. The difference could be attributed to the fact that in their models, failure was evaluated based on two different criteria: crack growth and plastic collapse, the smaller value is the predicted

failure pressure. The failure pressure due to crack growth mechanism is determined by a critical toughness, J_c, calculated from Charpy energy following Equation 30:

$$J_C = \frac{5(1-v^2)\sigma_Y}{E}\left(E_{CVN} - \frac{\sigma_{YS}}{20}\right) \tag{30}$$

The failure pressure due to plastic collapse mechanism is determined by a critical stress that is equal to 90% of the ultimate tensile strength. While in our models, the initiation of failure was predicted when the crack has penetrated the inner surface of the pipe, which is the same criteria as in Chapter 4.

5.3.2 Effect of Initial Crack Depth

Six XFEM models were developed with different initial crack depths to investigate the effect of initial crack depth (d_{cr}) on the failure pressure of a pipeline with CIC defects. The length of corrosion defect, length of crack defect, width of corrosion defect, and total defect depth were kept constant as 152.4 mm, 100 mm, 50.8 mm, and 3.81 mm, respectively. The total defect depth was kept as 60% of wall thickness and the initial crack depths considered for this investigation were 0%, 10%, 20%, 50%, 75%, and 100% of the total defect depth (d_T).

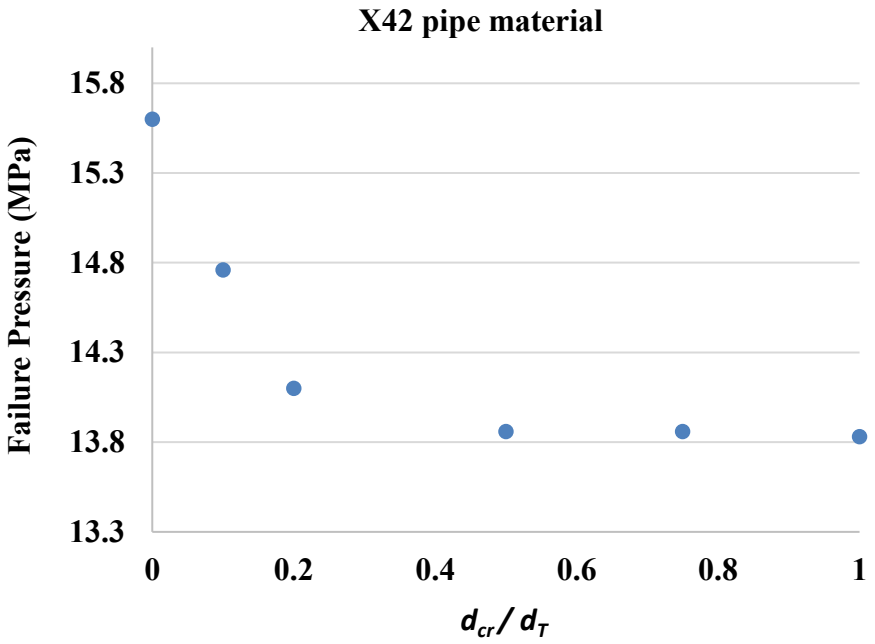

Figure 40: Failure pressure for different CIC defects with varying d_{cr}/d_T ratio (60%WT).

Figure 40 shows that the failure pressure decreases with the increase of initial crack depth. As expected, the failure pressure converges towards that of the long crack when the crack depth approaches the total defect depth. The failure pressure stabilized after the crack reached 50% of the total (crack plus corrosion) defect depth, thereby it can be deduced that the CIC defect could be treated as a crack defect when d_{cr}/d_T =0.5. As noted previously, CorLAS, RSTRENG, and LPC methods are commonly used to predict the failure pressure for crack-only and corrosion-only defects. Hence, the XFEM predicted failure pressures were then compared with the ones calculated based on CorLAS, RSTRENG, and LPC methods. It was found that for the corrosion-only defect, the predicted failure pressure (15.6 MPa) was closer to the one calculated using the LPC method (13.4 MPa) than RSTRENG method (9.56 MPa). For the crack-only defect, CorLAS method provided an estimate (12.03 MPa) that is 12% different from the one calculated using XFEM (13.8 MPa).

Later, the dependence of failure pressure on defect lengths was investigated. The total defect depth was 60%WT and the lengths of the crack and corrosion were twice the original values. Six XFEM models with different initial crack depths were simulated and it is interesting to note that the relationship between the initial crack depth and failure pressure was almost flat (Figure 41), implying that the initial crack depth would only influence the failure pressure for up to a certain defect length; if the defect length exceeds a particular value, the initial crack depth posed negligible influence on the failure pressure. Moreover, it was noted that when $d_{cr}/d_T = 0.5$, the scenario was the most severe with the lowest failure pressure. Since the difference between the CIC defect (when $d_{cr}/d_T = 0.5$), the crack-only defect, and the corrosion-only defect was less than 5%, implying that for any depth, the CIC defect could be treated as either a crack-only defect or a corrosion-only defect.

The predicted failure pressures of different methods (CorLAS, LPC, and RSTRENG) were compared with XFEM results. It was found that for the corrosion-only defect, the predicted failure pressure (11 MPa) was closer to the one calculated using the LPC method (11.16 MPa) with a difference of 1.4% than RSTRENG method (8.7 MPa) with 21% difference. For the crack-only defect, the predicted failure pressure (10.8 MPa) was close to the one using CorLAS method (11.78 MPa) with only 7% difference. Moreover, the failure pressures predicted by LPC and CorLAS were similar, therefore, for longer cracks, any CIC defect could be treated as either a crack-only or corrosion-only defect utilizing the available assessment method to eliminate the need for calibration with experimental results. It seems that analytical models are more accurate for predicting the failure pressure of pipelines containing longer cracks than shorter cracks.

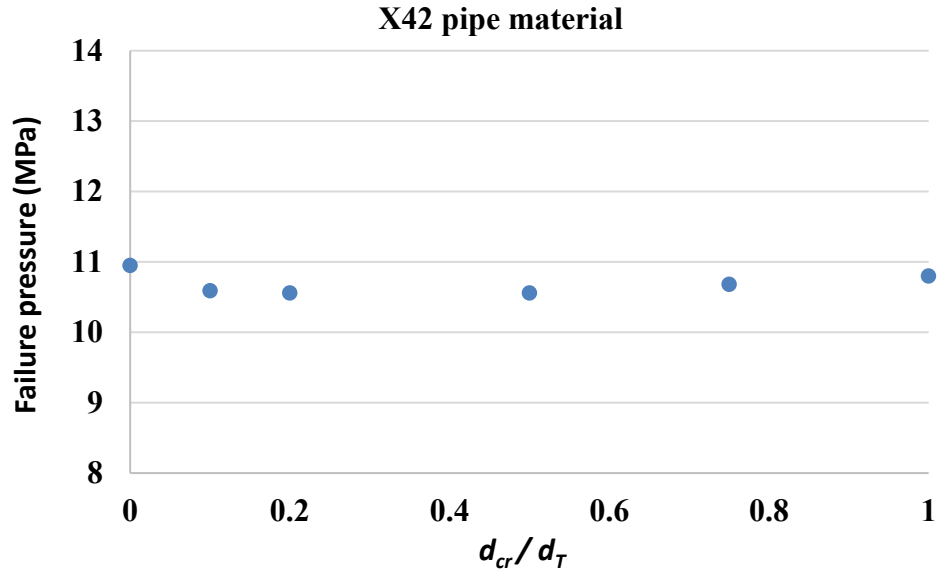

Figure 41: Failure pressure for CIC defects with varying d_{cr}/d_T ratio.

(when the defect lengths were twice the original value)

It is hypothesized that, given that failure in this study is defined as the pressure at which the crack propagates through the entire pipe wall thickness (i.e. crack depth extension of 2.538 mm which is the remaining ligament). Therefore, the change of failure pressure is more sensitive to crack extension behavior along the depth direction, as opposed to the length direction. The failure pressure increases if the crack propagates gradually in the depth direction (resembling a ductile failure mode), but it remains constant if the crack propagates suddenly in the depth direction (resembling a brittle failure mode).

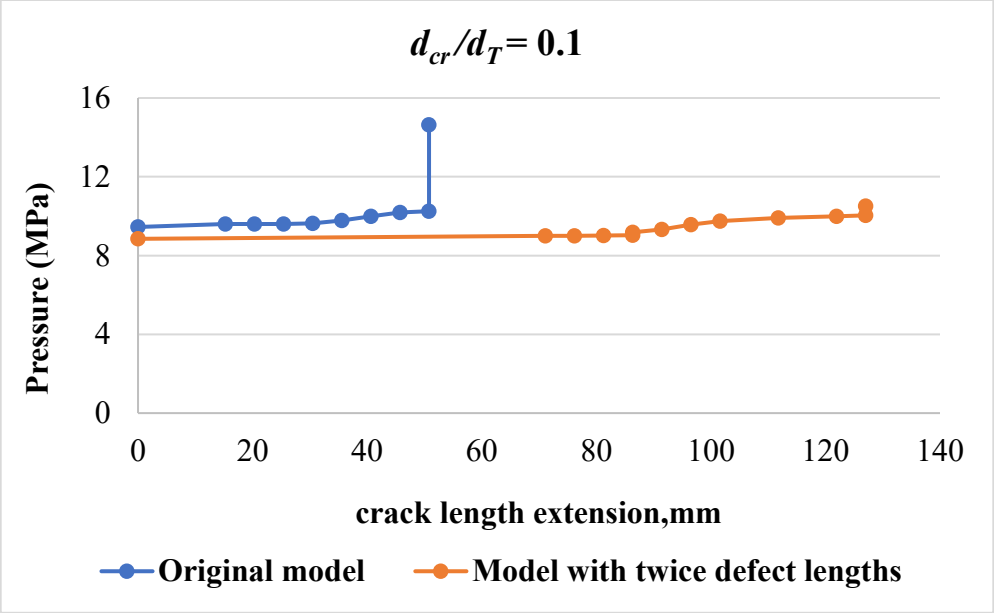

(a)

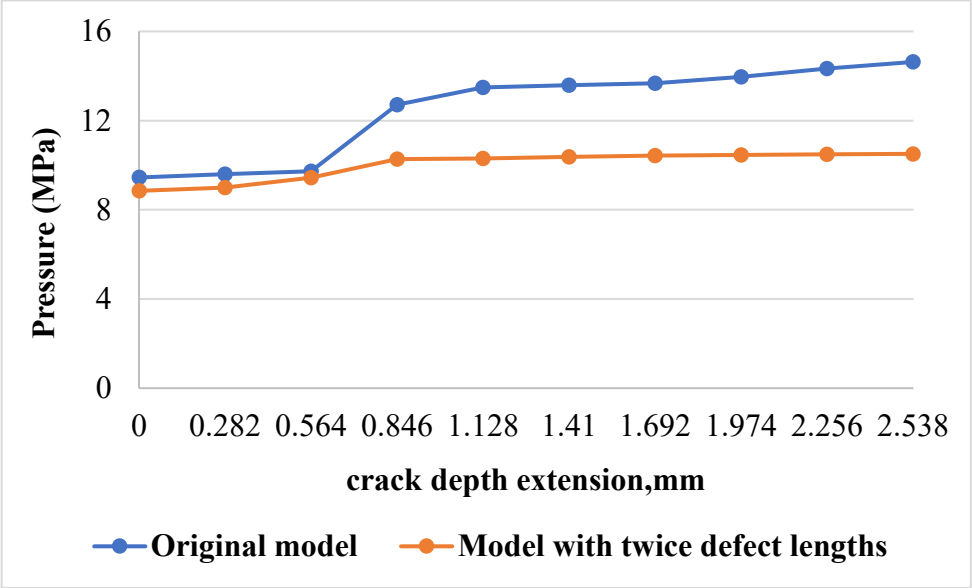

(b)

Figure 42: (a) The relationship between the pressure and the crack length extension; (b) The relationship between the pressure and the crack depth extension.

Figure 42 shows the variations of the pressure with crack extension in length and depth directions. The failure pressure of the original model is much higher than that of the model with twice the original value of crack and corrosion lengths. For the model with twice the lengths, it can be seen that the crack tends to firstly propagates through the length direction until a point, after that the crack propagates only through the depth direction. The crack depth extension jumps quickly from 1.128mm to 2.538mm (resembling a brittle failure mode), thus the failure pressure tends to be stabilized. However, as for the original model, the crack propagates gradually and in a more stable fashion in the depth direction (following a ductile failure mode), therefore the failure pressure increases gradually. It can be concluded that in the same material, the failure pressure will increase if the crack configuration leads to a more ductile behavior.

5.4 X52 Grade Results & Discussion

5.4.1 Model Validation

The same procedure as in the previous section is repeated here, the failure pressure of X52 pipe is predicted using the calibrated model from Chapter 4. The models are validated if the numerical results agreed with the burst test results from Ma et al. [20]. The full-scale tests were conducted on four specimens cut out from a 30-inch OD and 0.375-inch WT API 5L X52 line pipe that contained CIC defects. The corrosion defects, 152.4 mm long, 63.5 mm wide, were machined on the outer surface of the pipe with different depths (0%, 40%, 50%, and 55% of d_T), while the total defect depth was 55%WT. The experimental corrosion defect was achieved by mill grinding and the pipes were filled with water and pressurized to failure to determine the failure pressure. Failure pressures predicted using the XFEM model and the FE model were compared with the experimentally measured values (Figure 43).

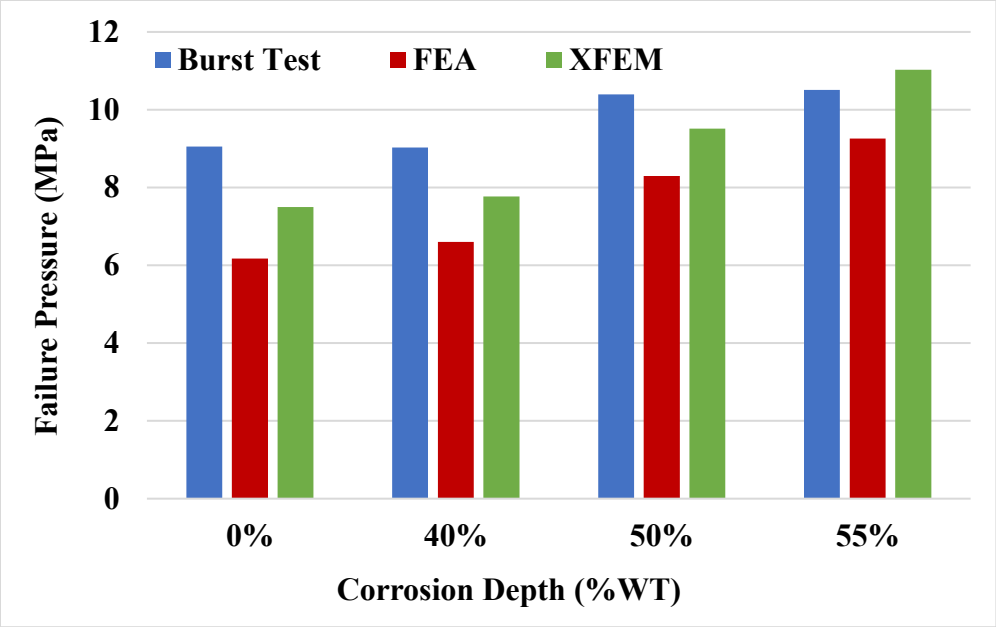

Figure 43: Comparison between XFEM, experimental, and FEA results for CIC modelling. FEA and experimental results were reported by Ma et al. [20].

The comparison of failure pressures from burst tests, FEA, and XFEM are illustrated in Figure 43. The FEA predictions reported by Ma et al. [20] are conservative compared to the test results as the predicted failure pressures are considerably lower than the experimental values. One of the reasons could be due to the difference of the shape of the crack of the FEA models reported by Ma et al. [20] and their experiments. In the tests, the shape of the crack is semi-elliptical, which exhibits higher failure pressure than the rectangular shape of crack that was simulated in Ma et al.'s work. By comparison, XFEM predictions are aligned with the experimental results with an error of approximately 5.8%, suggesting that XFEM can provide accurate predictions for failure pressures of CIC defects. Furthermore, the same set of damage parameters: M_{axpe} = 0.02 mm/mm and G_c = 150 N/mm were used to satisfactorily fit the experimental data, which indicated that this set of damage parameters could be used as the X52 pipe's parameter to predict the failure pressure of CIC defects.

5.4.2 Effect of Initial Crack Depth

Six XFEM models were developed with varying initial crack depths to investigate the effect of crack depth (d_{cr}) on the failure pressure of a pipeline with CIC defects. The length of corrosion defect, length of crack defect, and the total defect depth were kept constant as 152.4 mm, 100 mm, and 5.24 mm, respectively. The remaining ligament, b_o, was kept constant as 45% of wall thickness and the initial crack depths considered for this investigation were 0%, 10%, 20%, 50%, 75%, and 100% of the total defect depth (d_T).

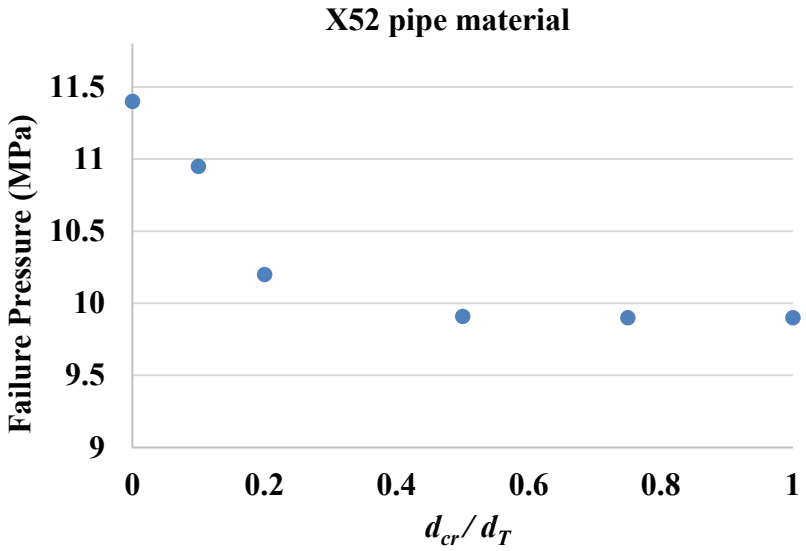

Figure 44: Failure pressure for CIC defects with varying d_{cr}/d_T ratio (d_T = 55%WT).

It was noted that the predicted failure pressure for a crack-only defect was lower than that for a corrosion-only defect and the failure pressure decreased nonlinearly with increasing the crack depth, as expected. Furthermore, the XFEM results indicated that the failure pressure for the CIC model tended towards that of the pure crack model when the crack depth was approximately 50% of the total defect depth.

Interestingly, the trend is similar with the one of X42 pipe material. This observation may lead to the inference that this trend is insensitive to pipe geometry and material properties, suggesting that the conclusions derived from this study may be applicable to a wide range of pipes. However, the investigation on X42 pipe material showed that this conclusion only applied to a particular length of defects, thus, it is assumed that for X52 pipe material, when the defect lengths exceeded a certain value, the initial crack depth may also have a negligible effect on the failure pressure.

The trend is consistent with our previous findings [73] where a numerical study was performed on full-scale X60 vintage pipes with cracks in corrosion defects under the effect of internal pressure, where the numerical model was validated using the experimental results obtained from Bedairi et al. [13]. Six XFEM models with different initial crack depths were analyzed to investigate how the depth of crack defect affects the failure pressure of the pipeline containing CIC defects. It was found that the initial crack depth had a significant effect on the failure pressure when the initial crack depth was less than 50% of the total defect depth. However, when the defect lengths exceeded a certain value, the failure pressure may be insensitive to the initial crack depth as mentioned earlier.

CHAPTER 6: CONCLUSIONS AND FUTURE WORK

6.1 Conclusions

In this thesis, several 2D analyses of CIC defects in pipelines had been conducted to predict the failure pressure of CIC defects using XFEM. In order to study the mesh size sensitivity in elastic-only and elastic-plastic materials, several models were built in which the length and width of the elements at the crack tip were changed. It was found that $l_h \times l_t$= 0.37 mm × 0.55 mm and $l_h \times l_t$ = 0.5 mm × 0.67 mm were the optimum mesh sizes for elastic-only material model and elastic-plastic material model, respectively.

After the optimum mesh size was determined, the effect of different CIC parameters on the failure pressure was investigated. Five CIC defects with different initial crack depths (ranging from 0.5 mm to 5 mm) were evaluated. For the elastic-only model which the failure pressure first decreased significantly with the increase of the initial crack depth, then the model exhibited a stabilization of the failure pressure when the ratio of the initial crack depth to the total defect depth (d_{cr}/d_T) was more than 0.5. Unlike the elastic-plastic model, the predicted failure pressure continued to decrease slightly with the increase of the initial crack depth, and it was found that the failure pressure for a CIC defect was bound between a crack-only defect and a corrosion-only defect. Three CIC defects with different corrosion widths (10 mm, 15 mm, and 20 mm) were evaluated, and as the value of the corrosion width increased, only a slight increase in the failure pressure was observed in both models, indicating that the corrosion width has little impact on the failure pressure. Two CIC defects with different corrosion profiles (semi-elliptical and semi-rectangular) were evaluated. The predicted failure pressure corresponding to the semi-elliptical corrosion profile is slightly higher

than that corresponding to a rectangular profile which can be inferred that the circumferential corrosion defect profile posed little effect on the failure pressure.

Next, a suitable set of XFEM damage parameters, M_{axpe} and G_c was calibrated and verified by matching the XFEM model predictions with the experimental results from [13]. Five CIC models were evaluated in 3D, and a good agreement was observed between the XFEM prediction results and the experimental data with an average error of 5.87%, which was much lower than the previously reported FE models predictions with an average error of 17.4%. The XFEM damage parameters were calibrated to be M_{axpe} = 0.02 mm/mm and G_c = 150 N/mm.

A numerical investigation of the effect of d_{cr}/d_T on the failure pressure was undertaken by analyzing six more CIC models with the same pipe dimension but with a wider range of d_{cr}/d_T ratios (varying from 0 to 1). It was noted that the predicted failure pressures decreased with the increase in the initial crack depth, with the decreasing trend stabilizing when the initial crack depth was more than 50% of the total defect depth.

RSTRENG, LPC, and CorLAS Version 2.0 were used to predict the failure pressure to examine the versatility of each method, and these analytical predictions were compared against the results with XFEM predictions. The results showed that for corrosion defect, the LPC method provided more accurate failure pressure prediction than the RSTRENG method. For crack-like defect, CorLAS provided comparable result to the XFEM prediction.

Lastly, the numerical study was performed on API 5L X42 and X52 vintage pipes with CIC defects under the effect of internal pressure. The calibrated model from chapter 4 was used to predict the failure pressure and the numerical models were validated using the burst tests results extracted from [20]. It was found that the predictions agreed well with the experimental results, meaning a critical value of M_{axpe} = 0.02 mm/mm and G_c = 150 N/mm could be successfully used in XFEM models for assessing the failure pressure in X42 and X52 pipe materials. This finding could serve as a good basis in effectively predicting the failure pressure of pipelines with various steel grades using XFEM.

For each pipe, six XFEM models were developed with different initial crack depths to examine the effect of initial crack depth on the failure pressure. It was found that the failure pressure decreased nonlinearly with the increase of the initial crack depth. In addition, the predicted failure pressure converged towards that of a crack-only defect when the crack depth was significant (greater than a critical value of 50% of the total defect depth). This observation would suggest that for shorter cracks, any CIC defect could be treated or analyzed as a crack-only defect after the crack depth reaching that critical value.

The dependence of the failure pressure on the defect length has been investigated by developing a CIC model where the lengths of corrosion and crack were taken as 304.8 mm and 101.6 mm, respectively. It was found that the curve of the failure pressure vs the ratio of d_{cr}/d_T was almost flat. It could be concluded that the initial crack depth only affects the failure pressure when the defect length is up to a certain value. If the defect length exceeds this value, the failure pressure is

insensitive to the initial crack depth and the CIC defect could be treated as either a crack or corrosion utilizing the current assessment methods to eliminate the need for calibration.

The overall results show that XFEM is as accurate and as effective as the best analytical models available and can successfully be used for the assessment of failure pressures of CIC defects in pipelines.

6.2 Recommendations and Future Work

While this study has demonstrated application of evaluating cracks in corrosion using XFEM, the models in this study still have some limitations. Currently, the damage initiation criterion assumes a fixed value as the critical maximum principal strain. It is recommended to develop a variable fracture criterion in the future studies, for example, fracture strain as a function of stress triaxiality using the Abaqus user subroutines.

Furthermore, this research did not investigate all the defect types that could be found on a pipeline. It is also recommended to examine the behaviour of different combinations of defects such as cracks within dents and circumferential cracks in girth welds.

For future work, the pipe could be modelled as the combination of solid part and shell parts using the shell-to-solid coupling to reduce the computational cost. Moreover, considering that all the current studies were focusing on low grade pipes, future research could further examine the applicability of the calibrated models on high grade pipes.

REFERENCES

[1] Mondal, B.C. (2018). Remaining strength assessment of deteriorating energy pipelines. PHD Thesis. Memorial University of Newfoundland.

[2] Guo, B., Song, S., Ghalambor, A., and Lin, T.R. (2014). Offshore pipelines: Design Installation and Maintenance. Second Edition. Gulf Professional Publishing, Elsevier.

[3] Zhang, X.F., Okodi, A., Tan, L.C., Leung, J.Y., and Adeeb, S. (2020). Forthcoming. Failure pressure prediction of crack in corrosion defects in 2D by using XFEM. PVP 2020-21046, Proceedings of the 18th Pressure Vessel Piping Conference, Minnesota, USA.

[4] Hosseini, A. (2014). Assessment of Crack in Corrosion Defects in Natural Gas Transmission Pipelines. PHD Thesis. University of Waterloo.

[5] Alberta Energy Regulator, https://www.aer.ca/protecting-what-matters/holding-industry-accountable/industry-performance/pipeline-performance.html, June 2019.

[6] Han, C.J., Zhang, H., and Zhang, J. (2016). Failure Pressure Analysis of the Pipe with Inner Corrosion Defects by FEM. International Journal of Electrochemical Science. 11(6): 5046-5062.

[7] Escoe, A. K. (2006). Piping and Pipeline Assessment Guide, Elsevier, New York.

[8] Fu, B., and Batte, A. D. (1998). Advanced methods for the assessment of corrosion in linepipe. Summary Report OTO 97065, UK Health and Safety Executive, London.

[9] Hassanien, S. S. A, and Adeeb, S. (2006). Probabilistic-Based Assessment of Corroded Pipelines: A Comparison Between Closed Form and Surrogate Limit States. IPC 2006-10247 proceedings of the 11th International Pipeline Conference. Calgary, Alberta, Canada.

[10] American Petroleum Institute, API 579. (2000). Recommended Practice for Fitness for Service.

[11] British Standards Institute, BS 7910, (2000). Guide on Methods for Assessing the Acceptability of Flaws in Metallic Structures. BSI-10.

[12] Jaske, C.E. (2010). CorLAS User manual. Version 2.25.

[13] Bedairi, B., Cronin, D., Hosseini, A., Plumtree, A. (2012). Failure prediction for crack-in corrosion defects in natural gas transmission pipelines. International Journal of Pressure Vessels and Piping. Volume 96-97, 90-99.

[14] Henshell, R.D., and Shaw, K.G. (1975). Crack tip finite elements are unnecessary*. International Journal of Numerical methods in Engineering, Volume 9, 495-507.

[15] Melenk, J.M, Babuska, I. (1996). The partition of unity finite element method: Basic theory and applications. Computer methods in Applied mechanics and Engineering. Volume 139, 289-314.

[16] Moes, N., Dolbow, J., and Belytschko, T. (1999). A finite element method for crack growth without remeshing". International Journal of Numerical methods in Engineering, Volume 46, 131-150.

[17] Fries, T.P., and Belytschko, T. (2000). The extended / generalised finite element method: An overview of the method and its applications. International Journal of Numerical methods in Engineering. 84(3): 253-304.

[18] Rege, K., Lemu, H.G. (2017). A review of fatigue crack propagation modelling techniques using FEM and XFEM. IOP Conference Series: Materials Science and Engineering. 276 (1), 012027.

[19] Dassault Systèmes. (2019). Abaqus Analysis User's Guide [Computer software]. Providence, RI : Dassault Systèmes Simulia Corp.

[20] Ma, J., Zhang, F., Tuggle, J. Assessment of Fitness-for-Service for Crack-in-Corrosion (CIC) Defects. Pipeline research council international draft report, 2018.

[21] API Specification 5L (2018). Specification for line pipe (46th ed.). Washington, DC: American Petroleum Institute (API).

[22] Astteris. https://atteris.com.au/pipeline-defect-assessment/, April 2017.

[23] Kim, Y.S., and Kim, J.G. (2018). Failure analysis of a thermally insulated pipeline in a district heating system. Engineering Failure Analysis. Volume 83, 193–206.

[24] Mouritz, A.P. (2012). Introduction to aerospace materials. Woodhead Publishing.

[25] Ahmad, Z. (2006). Principles of corrosion engineering and corrosion control. Butterworth-Heinemann.

[26] Popoola, L.T., Grema, A.S., Latinwo, G.K. et al. (2013). Corrosion problems during oil and gas production and its mitigation. International Journal of Industrial Chemistry. Volume 4, 1-15.

[27] Baker, M. (2008). Pipeline corrosion. U.S. Department of transportation pipeline and hazardous materials safety administration. Final report.

[28] Polasik, S. J., Jaske, C. E., and Bubenik., T. A. (2016). Review of engineering fracture mechanics model for pipeline applications. Proceedings of the 11th International Pipeline Conference. Volume 1: Pipelins and Facilities Integrity. Calgary, Alberta, Canada.

[29] Beavers, J. A., and Harle, B. A. (2001). Mechanisms of High-pH and Near-Neutral-pH SCC of Underground Pipelines. Journal of Offshore Mechanics and Arctic Engineering. 123(3): 147–151.

[30] Corrosion costs and preventive strategies in the united states. Report of National Association of Corrosion Engineers (NACE).

[31] Stack, M.M., Abdulrahman, G.H. (2010). Mapping erosion-corrosion of carbon steel in oil exploration conditions: some new approaches to characterizing mechanisms and synergies. 43 (7):1268-1277.

[32] Tanuma, T. (2017). Advances in steam turbines for modern power plants. Woodhead Publishing.

[33] Farotade, G.A., Popoola, P.A., and Popoola, O.M. (2016). Computational analysis of system and design parameters of electrodeposition for marine applications. Applied studies of costal and marine environments.

[34] Isecke, B., Schütze, M., Strehblow, H.H. (2011). Springer Handbook of Metrology and Testing. Springer Handbooks. Springer, Berlin, Heidelberg.

[35] James, B., Hudgins, A. (2016). Failure analysis of oil and gas transmission pipelines. Handbook of materials failure analysis with case studies from the oil and gas industry.

[36] Abu, R. (2011). Structural behaviour of dented pipelines. PHD Thesis. University of Windsor.

[37] Alang, N.A., Razak, N.A., and Zulfadli, M.R. (2013). The influence of gouge defect on failure pressure of steel pipes. IOP Conference Series: Material Science and Engineering. 50(1).

[38] ASTM E8/E8M-11.(2011). Standard test methods for tension testing of metallic materials. West Conshohocken, PA: American Society of Testing and Materials.

[39] Davis, J. R. (2004). Determination of yield strength for non-prestressed steel reinforcement. Tensile testing (2nd ed). Materials Park, OH: American Society for Metals (ASM International). Final draft report.

[40] CORROSIONPEDIA. https://www.corrosionpedia.com/definition/1126/ultimate-tensile-strength-uts. Accessed on March 22, 2018.

[41] Wiederhorn, S.M.(1991). Concise encyclopedia of advanced ceramic materials.

[42] Anderson, T.L. (2005). Fracture mechanics - Fundamentals and Applications. CRC Press, Taylor & Francis Group, Boca Raton, third edition.

[43] Blackman, B.R.K. (2011). Fracture Tests. In: da Silva L.F.M., Öchsner A., Adams R.D. (eds) Handbook of Adhesion Technology. Springer, Berlin, Heidelberg.

[44] Davis, J. R. (Eds.) (2004). Tensile testing (2nd ed). Materials Park, OH: American Society for Metals (ASM International).

[45] Kiefner, J.F. (2008). Defect Assessment-Conclusion: Modified Ln-Secant Equation Improves Failure Prediction. Oil and Gas Journal.

[46] Hahn, G.T., Sarrate, M., and Rosenfield, A.R. (1969). Criteria for crack extension in cylindrical pressure vessels. International journal of fracture mechanics. 5(3):187-210.

[47] Okodi, A., Lin, M., Nader, Y.G., Kainat, M., Hassanien, S., and Adeeb, S. (2020). Crack propagation and burst pressure of longitudinally cracked pipelines using extended finite element method. International Journal of Pressure Vessels and Piping. Volume 184.

[48] Cronin, D.S., and Plumtree, A. (2007). Assessment of Crack in Corrosion Defects in Natural Gas Transmission Pipelines. Confidential report to TCPL, November 30.

[49] Jaske, C.E. CorLAS User Manual, 2010, Version 2.25.

[50] Shih, C., and Hutchinson, J. (1976). Fully Plastic Solutions and Large Scale Yielding Estimates for Plane Stress Crack Problems. Journal of Engineering Materials and Technology. 98 (4): 289-295.

[51] Clough, R.W. (1960). The finite element method in plane stress analysis. In: Proceedings, 2nd Conference on Electronic Computation, A.S.C.E. Structural Division, pp. 345–378.

[52] Dowling, N. (2007). Mechanical behavior of materials. 3rd ed. Pearson Education.

[53] Belytschko, T., Moes, N., Usui, S., and Parimi, C. (2001). Arbitrary discontinuities in finite elements. International Journal for Numerical methods in Engineering. Volume 50, 993-1013.

[54] Abaqus 2019 Documentation. Dassault Systèmes.

[55] Zhang, Y. M., Fan, M., Xiao, Z. M., and Zhang, W. G. (2016). Fatigue analysis on offshore pipelines with embedded cracks. Ocean Engineering. Volume 117, 45–56.

[56] Liu, P. F., Zhang, B. J., and Zheng, J. Y. (2012). Finite element analysis of plastic collapse and crack behavior of steel pressure vessels and piping using XFEM. Journal of Failure Analysis and Prevention. 12(6), 707–718.

[57] Hojjati-Talemi, R. (2016). Numerical simulation of dynamic brittle fracture of pipeline steel subjected to DWTT using XFEM-based cohesive segment technique. Frattura ed Integritá Strutturale (Fracture and Structural Integrity). Volume 36, 151–159.

[58] Hojjati-Talemi, R., Cooreman, S., and Van Hoecke, D. (2016). Finite element simulation of dynamic brittle fracture in pipeline steel: A XFEM-based cohesive zone approach. Proceedings of the Institution of Mechanical Engineers, Part L: Journal of Materials: Design and Applications, 0(0), 1–14.

[59] Lin, M., S. Agbo, D.-M. Duan, J. J. R. Cheng, S., and Adeeb. (2020). Simulation of crack propagation in API 5L X52 pressurized pipes using XFEM-based cohesive segment approach. Journal of Pipeline System Engineering Practice.11(2):04020009.

[60] Hosseini, A., Cronin, D., and Plumtree, A. (2013). Crack in corrosion defect assessment in transmission pipelines. Journal of Pressure Vessel Technology. 135(2), 021701-1.

[61] Mok, D.H., Pick, R.J., Glover, A.J., and Hoff, R. (1991). Bursting of Line Pipe with Long External Corrosion. International Journal of Pressure Vessels and Piping. Volume 46, 195-215.

[62] Cronin, D.S. (2000). Assessment of Corrosion Defects in Pipelines. PHD Thesis. University of Waterloo.

[63] Ma, B., Shuai, J., Liu, D., and Xu, K. (2013). Assessment on failure pressure of high strength pipeline with corrosion defects. Engineering Failure Analysis. Volume 32, 209-219.

[64] Cronin, D.S., and Plumtree, A. (2008). Assessment of Crack in Corrosion Defects in Natural Gas Transmission Pipelines. Proceedings of the 7th International Pipeline Conference, Calgary, Canada.

[65] Munjiza, A., and John, NWM. (2002). Mesh size sensitivity of the combined FEM/DEM fracture and fragmentation algorithms. Engineering Fracture Mechanics. 69(2):281-295.

[66] Schwalbe, K.-H., Scheider, I., and Cornec, A. (2013). Guidelines for applying cohesive models to the damage behaviour of engineering materials and structures. SpringerBriefs in Applied Sciences and Technology, Springer.

[67] Agbo, S., Lin, M., Ameli, I., Imanpour, A., Duan, D., Cheng, J.J., and Adeeb, S. (2019). Evaluation of the Effect of Internal Pressure and Flaw Size on the Tensile Strain Capacity of X42 Vintage Pipeline Using Damage Plasticity Model in Extended Finite Element Method (XFEM). PVP 2019-94005 proceedings of the .Volume 5: High-Pressure Technology, San Antonio, Texas, USA.

[68] Mondal, B.C., and Dhar, A.S. (2019). Burst pressure assessment of corroded pipelines using fracture mechanics criterion. Engineering Failure Analysis. Volume 104, 139-153.

[69] Mondal, B.C., Dhar, and A.S. (2018). Improved Folias factor and burst pressure models for corroded pipelines. Journal of Pressure Vessel Technology. 140 (1), 011702–011711. ASME.

[70] ASME, 2009. Manual for determining the remaining strength of corroded pipelines: supplement to ASME B31code for pressure piping. American Society of Mechanical Engineers, New York, Standard No. B31G-2009.

[71] G. Fekete, and L. Varga. (2012). The effect of the width to length ratios of corrosion defects on the burst pressures of transmission pipelines. Engineering Failure Analysis. Volume 21, 21–30.

[72] Polasik, Steven J., Jaske, Carl E., and Bubenik, Thomas A. (2016). Review of Engineering Fracture Mechanics Model for Pipeline Applications. Proceedings of the 11th International Pipeline Conference. Volume 1: Pipelines and Facilities Integrity. Calgary, Alberta, Canada.

[73] Zhang, X.F., Okodi, A., Tan, L.C., Leung, J.Y., and Adeeb, S. (2020). Forthcoming. Failure pressure prediction of crack in corrosion defects using XFEM. IPC 2020-9312, Proceedings of the 18th Internal Pipeline Conference, Calgary, Canada.